Advanced Carbon Capture for steel industries integrated in CCUS Clusters

Innovation Action

This project has received funding from the European Union's Horizon 2020 research and innovation programme under the Grant Agreement No 884418.

D2.5 Experimental results from the TRL7 CASOH pilot: screening test results and tuned reactor models

Work Package: 2
Due date of deliverable: month 30
Reviewed due date of deliverable after project extension: month 55
Actual submission date: 5 /November /2024
Start date of project: 1st April 2020
Duration: 48 months (60 month after project extension)
Lead beneficiary for this deliverable: CSIC
Main Contributors: José Ramón Fernández (CSIC), Mónica Alonso (CSIC), Miriam Díaz (CSIC), Roberto García (CSIC), Alberto Méndez (CSIC), Marcos Cano (AM R&D), Alejandro Lengomin (AM R&D), Irene Alzueta (AM R&D), Carlos Abanades (CSIC)
Reviewer: Vincenzo Spallina (UNIMAN)
Dissemination level: PU

Contents

1. Version log 3
2. Definition and acronyms 4
3. Summary of the Report 5
4. Introduction and scope 7
5. CASOH TRL7 pilot plant description and experimental commissioning works 8
6. Screening operating conditions at TRL7 17
7. Tuning reactor model to TRL7 results 44
8. Conclusions 50
9. Bibliography / References 50
10. ANNEXES 53

*This project has received funding from the European Union's Horizon 2020 research and innovation programme under the Grant Agreement No **884418***

1. Version log

Version	Date	Released by	Nature of Change
0.1	10/09/2024	Carlos Abanades	Scope and first draft
0.2	27/09/2024	V Spallina	Reviewed draft
0.3	5/10/2024	JR Fernandez/M Alonso/M Díaz	Integrated draft with all contributions
1.0	5/11/2024	R Porter	Final version

*This project has received funding from the European Union's Horizon 2020 research and innovation programme under the Grant Agreement No **884418***

2. Definition and acronyms

Acronyms	Definitions
BFG	Blast Furnace Gas
CASOH	Calcium Assisted Steel-mill Off-gas Hydrogen
LHV	Lower Heating Value
TGA	Thermo-gravimetric Analysis
WGS	Water Gas Shift
TRL	Technology Readiness Level
CaL	Calcium Looping
SCM	Shrinking Core Model

*This project has received funding from the European Union's Horizon 2020 research and innovation programme under the Grant Agreement No **884418***

3. Summary of the Report

This public deliverable reports the first test and experiments carried out on the CASOH pilot, from the end of the commissioning works marked by D2.4 ("Factory acceptance test", delivered in Nov 2023) to the beginning of September 2024. The new pilot was built at the *GasLab* site of the ArcerlorMittal R&D, in the plant of Asturias (ES), to test at TRL7 the CASOH process *("Calcium Assisted Steel-mill Off-gas Hydrogen production"*) under development in the C^{4}U project to decarbonise Blast Furnace Gases (BFG). The pilot has entered operation after severe delays in the commissioning works initiated soon after the COVID pandemic, due to the challenges characteristic of building these kinds of TRL6-7 pilot scales. Most of the initial testing hours operating the integrated CASOH pilot were still devoted to carry adjustments on the pilot equipment and instruments, re-calibrations, solve gas leaking problems under increasingly demanding testing conditions (i.e. temperatures, use of fuel gases), repair elements damaged during first high temperature trials (i.e. a broken gas preheater and malfunctioning gaskets) and solve communication problems and logic issues between components and instruments (i.e. torch, compressor etc) and the control system, necessary to carry out safe operations in the pilot. The Annex to this report provides a chronological description of such works and problems during first operations, as it may be useful for other developers of TRL6-7 pilots. The initial operations led to a first fully successful experiment in May 2024 achieving a first decarbonisation of BFG. The main body of this report refers to the dynamic test conducted to demonstrate for the first time at TRL7 all reaction stages of the CASOH process. As anticipated in the DoW of the C^{4}U project, these first test have been carried out under dynamic conditions, and with a limited quantity of Ca/Cu materials in the bed of solids (about 100kg of $CaCO_3$, provided by Carmeuse well mixed with 100 kg or Cu-supported catalyst supplied by Johnson Matthey). These solids form a bed of just about 1 m bed height. Future test on more steady state conditions and taller bed heights (< 5 m set at maximum in the design of the reactor) will be reported in Deliverable D2.7 at the end of the project.

A first experiment involving gas-solid reactions in the CASOH pilot was the activation of the bed of solids by calcining part of the $CaCO_3$ to CaO and the reduction of CuO to Cu using the CO and H_2 contained in the BFG. For safety reasons, and to gain confidence on pilot operability, the calcination was carried out using only the thermal power available from the electric preheater of the pilot (i.e. supplying air or N_2 at 700°C to the bed of solids) and the CuO reduction was conducted at relatively mild temperatures (about 400°C), before calcination. The first full CASOH reaction stage was achieved in June 2024, with BFG and steam entering the pre-calcined reactor containing about 5% active CaO and the reduced Cu catalyst. The behaviour of the reactor was "as expected" from earlier test at lower TRL under the same conditions: a first breakthrough in gas compositions is observed, with rapidly increasing concentrations of H_2

This project has received funding from the European Union's Horizon 2020 research and innovation programme under the Grant Agreement No ***884418***

measured at the exit of the reactor (reaching over 40%v H_2 and capture efficiency of 98% due to the favourable conditions for carbonation and water gas shift enhanced reactions), followed by a second breakthrough that takes all gas concentrations to values characteristic of the WGS equilibrium. Such breakthrough in gas compositions marks the end of the active CaO in the bed (because of its carbonation to $CaCO_3$). Subsequent steps of Cu oxidation with air and CuO reduction with BFG also follow the expected breakthrough changes in concentration of O_2 and CO_2. All product gases are diluted in these first test, due to the need for safety reasons to maintain a N_2 feed through the electric gas preheater. The observed gas concentration trends and temperature profiles in the bed during these full cycle test are qualitatively consistent with previous test carried out at CSIC and UNIMAN in lower TRL rigs, with the same materials and reactors. Indeed, we re-visit in this deliverable the reactor model developed in the C^{4}U project (see details in D2.3) to interpret and scale up the available results at TRL7 from CASOH reaction stages described in this report. This represents an important milestone in the validation of the reactor model develop for the CASOH process, because a reasonable agreement of predictions vs experimental results is observed. Such model validation (from TRL3 to TRL7) provides sufficient confidence for imminent experiments involving taller beds (3-4 m of bed material, to be reported in D2.7), longer duration and higher number of cycles, that will be carried in during the next few months until the end of the C^{4}U project in March 2025.

Therefore, the main achievements reported in this deliverable D2.5 are:

- Complete, safe and successful operation of the TRL7 CASOH pilot for the first time, accumulating 550 h of valuable operation experience. Using a first batch of 200 kg of well mixed Ca and Cu commercial solid particles to undertake, under dynamic conditions, a first demonstration of all the CASOH reactions stages for the first time.
- First decarbonisation of real BFG, producing a H_2-rich fuel product gas with over 40%v H_2 and less than 1% CO_2 (when correcting for the N_2 safety flow used to protect preheater) from the CASOH reaction stage.
- First validation of the CASOH reactor models with experimental data obtained at TRL7, providing confidence for reactor and process scale-up to be further validated during the remaining test planned until the end of the project.

*This project has received funding from the European Union's Horizon 2020 research and innovation programme under the Grant Agreement No **884418***

4. Introduction and scope

This public deliverable D2.5 is part of Work-package 2 of the C⁴U project [1]. The main objective in WP2 is the experimental demonstration at TRL7 of the CASOH process *("Calcium Assisted Steel mill Off-gas Hydrogen production"*) that is schematically represented in Figure 4.1 and is based on a high temperature solid looping process involving Ca and Cu functional materials [2,3]. This process is a CO_2 capture technology designed to produce H_2 and heat from steel mill off-gases that contain CO, such as BFG, which is today a major source of carbon (in the form of CO and CO_2) in integrated steel mills. The productive step of the process (the "CASOH" stage) relies on high-temperature and reversible carbonation/calcination reactions of $CaO/CaCO_3$, in the presence of a Cu-based Water Gas Shift catalyst. This allows the production of H_2 from the WGS reaction of steam of the CO contained in the BFG. The presence of CaO in the bed, allows the capture of the CO_2 contained in the BFG, as well as the CO_2 formed in the WGS reaction of CO with H_2O, displacing by Le Chaterlier´s principle all reactions towards the production of H_2.

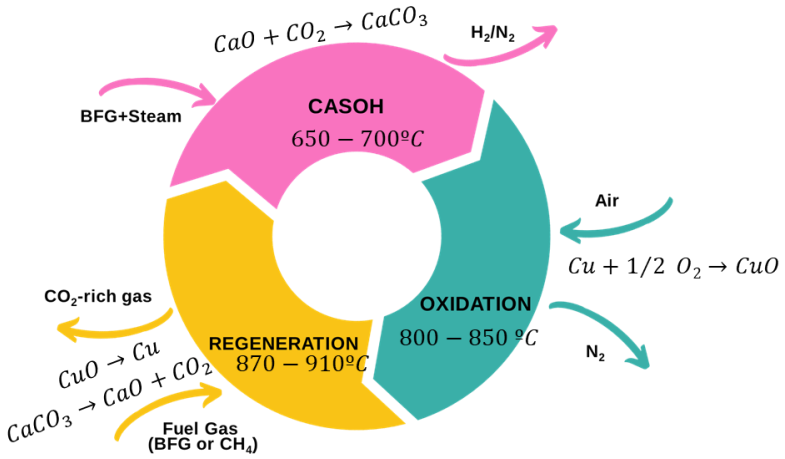

Figure 4.1 General scheme of the CASOH process as planned in the DoW of the C⁴U project (1).

Once that the packed bed is exhausted of active CaO (because CO_2 has been captured as $CaCO_3$) the reactor must enter additional reaction and heat removal stages to regenerate a bed of active CaO (and active Cu catalyst) while producing concentrated CO_2 during the decomposition of $CaCO_3$. To this end, the original CASOH concept as in Figure 1 was designed to use the exothermic reaction of reduction of CuO to Cu in consecutive oxidation-reduction stages. Enhanced versions of the CASOH process are currently being examined in WP3 by

This project has received funding from the European Union's Horizon 2020 research and innovation programme under the Grant Agreement No ***884418***

applying partial pressure swings on the carbonated bed of solids resulting after a CASOH stage (see Deliverable D2.6 and patent documents 7-8)

The experimental proof of concept at TRL≤4 for the CASOH process has been already published in the open literature by C⁴U project partners UNIMAN and CSIC (4-6), but it has remained a key objective of the C⁴U project to demonstrate at TRL7 the reactions involved in the CASOH process as shown in Figure 4.1. In this Deliverable 2.5, we report the commissioning works of a new TRL7 pilot built to demonstrate the CASOH process when treating BFG from the ArcelorMittal factory of Gijón (ES). The basic pilot design was almost completed at the end of 2021 [9] and works were initiated soon after to build it at the GasLab industrial R&D testing site located in said factory (see section 5). After several delays and shortcomings during commissioning works (see section 5 and Annex 10.1), the pilot has managed to generate in the first half of 2024 the first TRL7 results, relevant for all gas-solid reactions involved in the CASOH process (see section 6 and Annex 10.2). The experimental information disclosed in this report, corresponds to more than 550 h of commissioning and full testing campaign at high temperature that have allowed the tuning of the reactor model with TRL7 data. The same model had been used successfully to fit experimental data from TRL3-4 [5] and has required little modification to fit the new TRL7 data as described in section 7 and Annex 10.3.

Future work will extend the scope of the experiments to cover a wider range and longer duration experiments as anticipated in task T2.4, to complete the planned deliverable D2.7, and provide final proof of concept of the CASOH technology at TRL7.

5. CASOH TRL7 pilot plant description and experimental commissioning works

The detailed features of the CASOH pilot were described in D2.2. (September 2021) and its Addendum (June 2022), as well as in the congress publication [9]. During Executive Board meetings, internal progress reports and technical documents associated to the first and second Reporting Periods, we have reported important delays in WP2 activities associated to the commissioning works of the pilot, led by CSIC according to the DoW. The description of such deviations is outside the scope of this Deliverable.

Deliverable D2.4 (led by AM R&D: "Factory acceptance test results of the CASOH pilot") was submitted on the 1st of Nov 2023. This marked the acceptance of all physical elements and instruments, and their integration and assembly, allowing testing for the first time with integrated pilot. About 350 h of operating experience of the pilot between Nov 2023-March

*This project has received funding from the European Union's Horizon 2020 research and innovation programme under the Grant Agreement No **884418***

2024 were accumulated in test designed to set up operating and safety protocols, quantifying and correcting pressure drops and leakages in the reactor and other subsystems, re-commissioning BFG and Natural Gas combustion modes in the torch of the pilot, testing gas analysis and alarms with BFG and flue gases produced in the pilot, quantification of heat losses. Also, correcting multiple problems and malfunctions detected during these first tests with the integrated pilot. Several additional repairs by AM R&D and CSIC on the pilot and the control system have been needed, as well as few changes in the PFD by installing additional instruments and valves to improve safety and control of the pilot. All these efforts were directed to reach Milestone 8 (First H_2 from decarbonized BFG) at the beginning of May 2024 and Milestone 27 (Go/No-Go, achieved in June 2024). The following paragraphs provide a description of the CASOH pilot as finally commissioned by CSIC and AM R&D, and a summary of the works carried out towards the achievement of Milestone 8 and 27.
Figure 5.1 shows a screenshot of the final PFD of the CASOH pilot, as displayed on the control system screen. This PFD includes the equipment of the pilot, together with the supply lines of BFG, natural gas (NG) (for the CASOH operation and for the flare), steam and N_2, all of them obtained directly from the ArcelorMittal GasLab utilities network. Moreover, the air and CO_2 needed for the process are supplied by a compressor (COMP) and from pressurized cylinders, respectively. Finally, the PFD also contains the cooling water circuit for the reactor product gases and the gas sampling system connected to Analyser 1 and 2 for the measurement of gas composition at various points in the pilot.

BFG can be fed into the pilot by means of BLOWER 1 at a pressure of up to 4 bara, at a temperature near ambient conditions and saturated with water. BFG enters the pilot by opening the on/off valve V13. The flow of BFG is regulated by means of the insertion probe mass flow meter MF1 and the associated control valve FCV1 installed downstream. Moreover, the subsequent non-return valve NRV1 avoids the reverse flow in this BFG line. The pressure regulating valve PRV2 ensures that the pressure in this line never exceeds 1.5 bar, which is currently the maximum design pressure permitted in the gas preheaters (PREH), as explained in Addendum D2.2. During certain operations in the pilot, it is necessary to send BFG directly to the flare, bypassing the reactor. In this case, the on/off valve V17 (new in this PFD compared to previous versions) is closed, and the on/off valve V12 is opened, allowing the BFG to bypass the reactor and flow directly to the flare. The thermocouple T3 measures the temperature of the BFG (or NG) before it enters the reactor.

Moreover, the pressure safety valve PSV2 will send the gas to flare in case of overpressure in this line.
Since the preheaters (PREH) have no ATEX certification, they had to be located more than 1.5 m away from the entry point of BFG (and NG) to the reactor. As also detailed in Addendum D2.2, this distance has been gained by means of a two-meter refractory-lined pipe to connect PREH

*This project has received funding from the European Union's Horizon 2020 research and innovation programme under the Grant Agreement No **884418***

with the reactor inlet (not shown in the PFD for the sake of simplicity). The connection of BFG (and NG) line into this refractory pipe is made at a distance of 1.5 meters from the preheaters to comply with ATEX safety specifications. The non-return valve NRV3 avoids the reverse flow in this line.

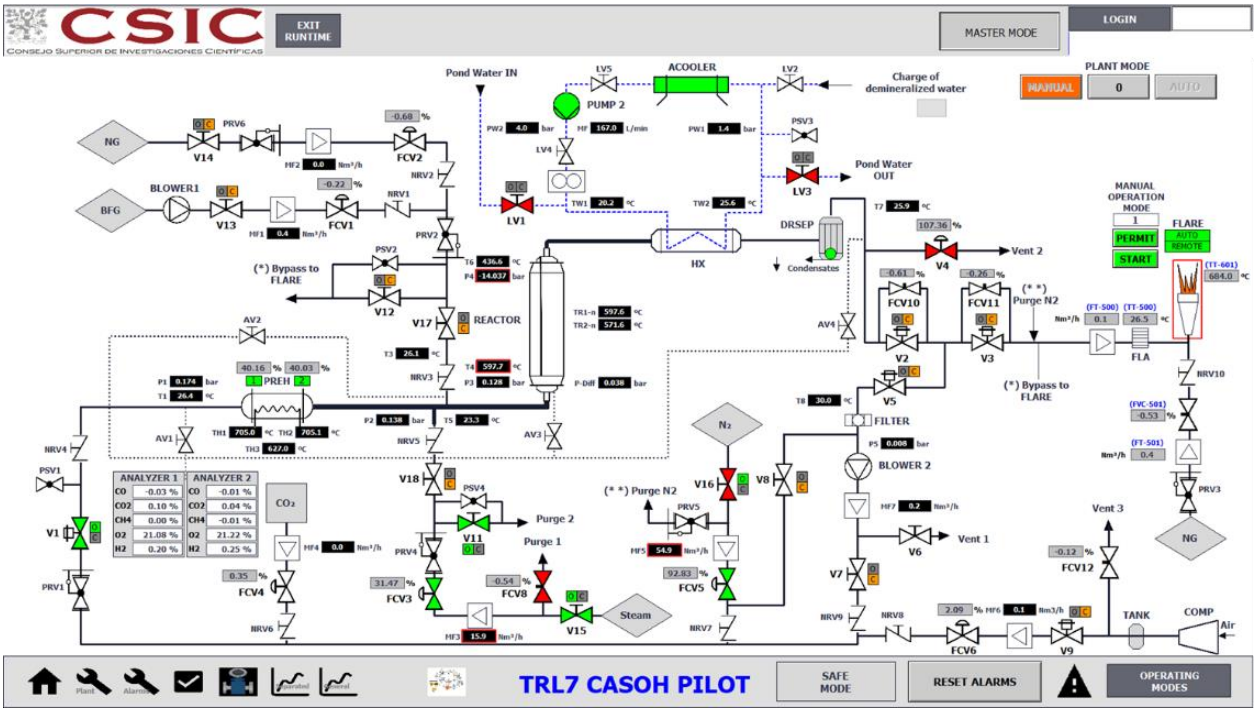

Figure 5.1 Final PFD diagram of the CASOH pilot as shown in the control room during pilot preheating with air.

On the other hand, steam is supplied from the AM R&D utility at around 150 °C and 2 bara, and can enter the pilot by opening the on/off valve V15. The flow control valve FCV8 is used to purge initially the line. To obtain a stable flow of steam during operation, the on/off valve V11 are initially open, whereas the flow of steam is regulated by means of the orifice plate flow meter MF3 and the associated control valve FCV3. Once a flow of steam through purge 2 without condensate is observed, FCV8 can be closed. Finally, to feed steam to the pilot the on/off valve 18 (new in this PFD compared to previous versions) must be open. The connection of the steam line into the refractory pipe is made close to BFG inlet, at a distance of 1.2 meters from the preheaters. The non-return valve NRV5 avoids the reverse flow in this line. The thermocouple T5 and the pressure sensor P2 measure the temperature and the pressure, respectively, of the steam circulating through this line.

*This project has received funding from the European Union's Horizon 2020 research and innovation programme under the Grant Agreement No **884418***

As mentioned above, the air required for the pilot operation (mainly during the copper oxidation stage and bed preheating) is supplied by a compressor (COMP) capable of delivering air at a pressure of up to 10 bara (however, note that high pressure is not to be tested within the C⁴U project). Downstream of the compressor, there is a 3000-liter buffering tank (TANK) to ensure a stable air flow during operation. There is an initial purge controlled by valve FCV12, which can be opened or closed towards vent 3 in case of overpressure in this section of the air line. The air enters the pilot by opening the on/off valves V9 and V1. The input of air to the pilot plant is regulated by means of the insertion probe mass flow meter MF6 and the associated control valve FCV6 installed downstream. Moreover, the subsequent non-return valves NRV8 and NRV4 avoids the reverse flow in this line of air. The pressure regulating valve PRV1 limits the maximum achievable pressure in this line at 1.5 bara. Moreover, the pressure safety valve PSV1 will purge gas in case of overpressure in this line. The thermocouple T1 and the pressure sensor P1 measure the temperature and the pressure, respectively, of the gas circulating through this line, before it enters the preheater (PREH).

From this point onwards, the gas can be preheated as it flows through two preheaters (PREH), which are arranged in parallel and have a combined total power of 80 kW (2x40kW), as detailed in Addendum D2.2. These preheaters have a maximum specification outlet temperature of 1100 °C, but the exit gas only can reach a maximum temperature of 700 °C due to the restrictive design temperature of the refractory-line pipe used to connect PREH with the reactor. The thermocouples TH1 and TH2 measure the temperature of the gas flowing through each preheater, whereas the thermocouple TH3 indicates the resulting temperature of the gas at the preheaters exit.

As mentioned above, the CO_2 needed for the process comes from pressurized cylinders. The input of CO_2 to the pilot plant is regulated by means of the insertion probe mass flow meter MF4 and the associated control valve FCV4. In this case, the subsequent non-return valve NRV6 will avoid the reverse flow in this line.

The supply of N_2 to the pilot plant is carried out by opening the on/off valve V16. This line splits into two pipes. One connects directly to the flare (N2 purge), as this equipment requires a supply of N_2 for its operation. The pressure regulating valve PRV5 limits the maximum achievable pressure in this line at 1.2 bara, according to flare specifications. The second pipe delivers the N_2 required for plant operations through the reactor. The flow of N_2 is regulated via the insertion probe mass flow meter MF5 and the associated control valve FCV5 installed downstream. Reserve flow in this line is avoided thanks to the non-return valve NRV7.

There are two natural gas (NG) inlets to the pilot. One provides the NG needed for plant operations through the reactor, while the other supplies the NG required for the flare. In both

*This project has received funding from the European Union's Horizon 2020 research and innovation programme under the Grant Agreement No **884418***

lines, the maximum pressure is controlled by the regulating valves PRV6 and PRV3, respectively. The NG for the process enters the pilot through the on/off valve V14, and the flowrate is controlled via the mass flow meter MF2 and the associated control valve FCV2. The subsequent non-return valve NRV7 avoids the reverse flow in the NG line.

In every stage of the CASOH process, the gas streams are fed into the bottom part of the packed-bed REACTOR, and the product gas leaves the reactor from the top. To measure the axial temperature along the reactor, three multipoint thermocouples are inserted into the bed, measuring temperature at 22 points throughout a fully loaded bed (i.e., TR1-10, TR2-10, T4, and T6). Moreover, pressure sensor P4 measures the pressure at the top of the bed, and the differential pressure sensor P-Diff records the pressure drop across the reactor during operation. The product gas after the reactor is directly introduced into the heat exchanger (HX), where it is cooled down to around 25-30 °C. Demineralized water is preferably used as cooling fluid in the heat exchanger HX. The charge of the demineralized water in the cooling circuit is carried out through the on/off valve LV2. The thermocouples TW1 and TW2 measure the temperature of the cooling water at the inlet and the outlet of the heat exchanger, respectively. The demineralized water circulates in a closed loop at a pressure of around 1.5 bara (measured in PW1), and it is refrigerated by means of the air cooler ACOOLER composed of 6 fans. PUMP 2 drives a flow of water of about 165 l/min, which is measured by means of the turbine flowmeter FM. Moreover, the pressure safety valve PSV3 will act in case of overpressure in the cooling circuit. In case of failure in the circulation of the demineralized water, the on/off valve LV1 is opened to feed pond water to the cooling circuit, which flows in an open circuit and is finally discharged through the on/off valve LV3. The pressure sensor PW2 measures the pressure in the pond water supply pipe. LV4 and LV5 are on/off valves that remain open at all times, except when the pump needs to be removed due to a malfunction. Only then, these valves will be closed, thereby avoiding the need to drain the entire water circuit.

The product gas after cooling is directed to the drop separator DRSEP to remove liquid water in the form of small droplets present in the gas and then meet the requirements for the downstream flare system. When the product gas is air, nitrogen, or CO_2 (or a mixture of them), it is released directly to vent 2 by opening the on/off valve V4. In the other cases (i.e. in presence of fuel gases), the product gas is finally sent to the FLARE for the controlled combustion. The on/off valves V3 and V5 are then open to allow the operation. Flow control valves FCV10 and FCV11 are installed in parallel to act in case of overpressure in the line caused by malfunction of V2 and/or V3.

The supply of natural gas to the FLARE (measured by FT-501) is regulated according to the measure from the mass flow meter FT-500, which ensures that valve FVC-501 opens

*This project has received funding from the European Union's Horizon 2020 research and innovation programme under the Grant Agreement No **884418***

appropriately to achieve proper gas combustion in the FLARE. The subsequent non-return valve NRV10 avoids the reverse flow in this NG line.

The pilot can also operate in a semi-closed loop of N_2 to accommodate the temperature of the packed-bed REACTOR (i.e. during Heat Removal stages). In that case, the on/off valves V2 and V5 are open, and the N_2 released from the reactor is directed to the BLOWER 2 in order to be re-compressed. A particle FILTER installed upstream of BLOWER2 retains the particles swept by the gas that could affect negatively the operation of the BLOWER2. The flow of N_2 is measured by the mass flow meter MF7. During heat removal stages the on/off valve V7 located downstream is open and the subsequent non-return valve NRV9 avoids the reverse flow in this N_2 line. The on/off valve V6 is normally closed unless a depressurization in this line is needed. Finally, a suitable feed of N_2 through the on/off valve V8 should avoid under-pressure in the BLOWER2 suction.

With respect to gas analysis, there are 4 sample points to measure gas composition before and after the reactor. All samples are transferred using PUMP1 from the corresponding sample point to the ANALYZER/S located in the analysis room through heat-traced silico-steel coated tubes. The on/off valves AV1-AV4 are operated manually to measure the gas composition at the different sample points.

Figure 5.2 provides various overviews of the pilot from different angles, including a view of the control room.

A key step in the commissioning works was the uploading to the reactor the Cu catalyst material manufactured by JM and the limestone batch selected and conditioned by Carmeuse for TRL7 testing. A detailed document was prepared by CSIC and AM R&D, with supervision from safety experts, to allow a safe operation involving the lifting of the head of the reactor, the lifting 7m over the head of the reactor of the temperature sensors to allow their introduction through the narrow fittings welded on the head of the reactor, their pass through the insulation layer and internals in the interior of the reactor and the charging of a 200 kg mixture of Ca/Cu solid materials. Some photographs of this operation are shown in Figure 5.3.

*This project has received funding from the European Union's Horizon 2020 research and innovation programme under the Grant Agreement No **884418***

Figure 5.2 Final overview of the CASOH pilot fully commissioned.

*This project has received funding from the European Union's Horizon 2020 research and innovation programme under the Grant Agreement No **884418***

Figure 5.3 Details of the uploading operation of solids (top) and temperature and gas analysis probes to the interior of the reactor (bottom)

*This project has received funding from the European Union's Horizon 2020 research and innovation programme under the Grant Agreement No **884418***

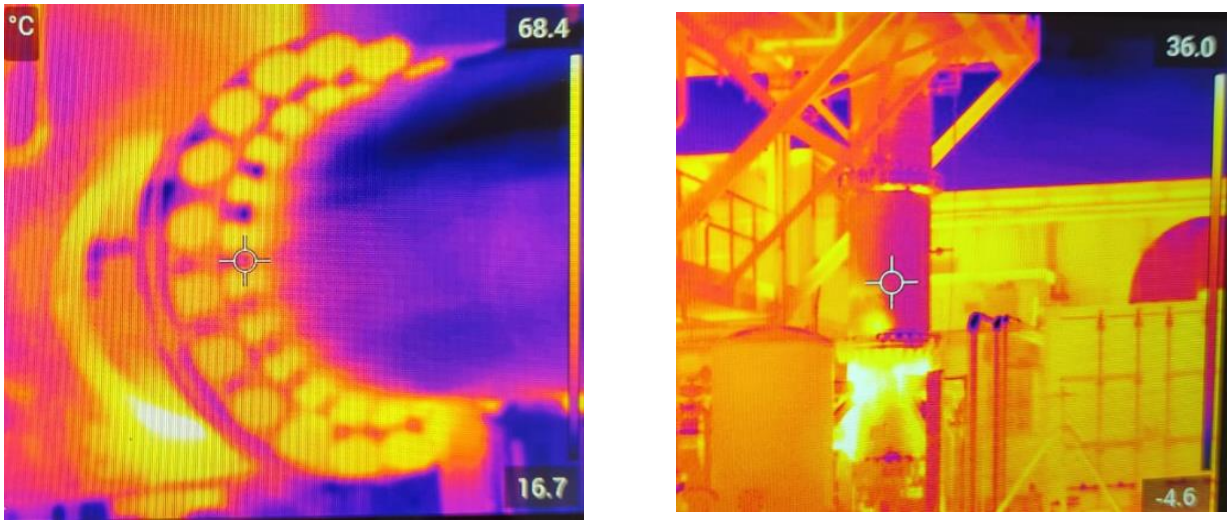

Figure 5.4 Detail of works to change reactor bolts (left) and external temperature mapping (central gas reactor inlet after preheater: right: overall reactor) during operation at high temperatures (as in Figure 5.1)

Operations on the pilot continued testing start up protocols, design checks and safety test, as described in more detail in Annex 10.1. In order to adapt to safety protocols and to the final design of the pilot, several changes in the start-up sequences were needed respect to what was originally planned in the DoW: the first heat up of the materials in the bed to about 600°C was carried out by using the electric preheaters (and not redox-reactions as planned in the DoW). Preheated air or N_2 up to 250 Nm^3/h was used for such purpose. During one of such start-ups towards high temperature conditions needed for the chemical activation of the solids, a malfunction in one of the gas preheaters was detected when going over 800°C (well below the maximum design temperature of the preheater stated by the manufacturer Khantal, theoretically up to 1100°C). After the eventual repair of the preheater the first hot test towards the activation (by calcination of $CaCO_3$ to CaO) of the batch of materials loaded to the reactor were carried out. Such test were also used to calibrate thermal insulation in the reactor, using a thermal analysis of the pilot with an infrared camera. These tests confirmed a high quality thermal insulation of the chemically active bed of solids (see Figure 5.4 right). These operations led to the eventual achievement of the first dynamic test experiments involving all relevant gas-solid reactions in the CASOH process, as described in the next section.

*This project has received funding from the European Union's Horizon 2020 research and innovation programme under the Grant Agreement No **884418***

6. Screening operating conditions at TRL7

As stated in the DoW, one of the main objectives of WP2 in the C⁴U project is to demonstrate the operation of the CASOH pilot for the H_2-N_2 production, in a real industrial environment by treating real BFG from the ArcelorMittal plant in Asturias (ES). The target is to accumulate more than 2000 h of operation experience, under realistic and relevant conditions, including the high temperatures and highly cycling operating conditions demanded by the CASOH process of Figure 1 (including as much as possible the enhanced CASOH process variants that have been proposed along the progress of the C⁴U project, that have been analysed and reported in WP3). As noted above, operation with the CASOH pilot has been initiated from the site or site acceptance test in November 2023, accumulating until the beginning of September 2024 about 550h of valuable operation experience, including the operations during commissioning works described in the previous section towards Milestone 8 and Milestone 27 and the first series of dynamic experiments. These will be used to screen operating windows and conditions for long duration experiments to be carried out from September 2024 and be reported in D2.7 (February 2025).

This section presents the examples of the most interesting and relevant part of the experiments conducted to date under highly dynamic conditions in the reactor, including all relevant gas-solid reactions playing a role in the CASOH process as outlined in Figure 1: CASOH, Cu oxidation, CuO reduction before/or during calcination and heat removal/supply stages. The tests have been conducted with different initial bed temperature profiles, gas residence times, gas composition inlets during CASOH stage (with and without steam) and during the calcination-reduction stages, O_2 contents during the Cu oxidation stage. More details of the experiments are given in graphical form in Annex 10.1 and 10.2.

To facilitate discussions, the figures used in this section will not include the model-fitted curves obtained when using the reactor model available to describe all reaction stages (see for that purpose next section 7 and in Annex 10.3).

6.1 Example of a CASOH reaction stage

As outlined above, the fixed-bed reactor was loaded with about 50 kg of alumina (Al_2O_3), which serves as the support and gas distributor for the reactive bed. On top of this, a mixture of 200 kg of the Ca- and Cu-based materials (pre-mixed in a 50% mass ratio) was added, forming a reactive bed height of 1 meter.

*This project has received funding from the European Union's Horizon 2020 research and innovation programme under the Grant Agreement No **884418***

Before proceeding with the CASOH stage described below, a partial calcination of $CaCO_3$ was conducted by feeding N_2 at an inlet temperature of 750ºC. During this operation, the degree of calcination was monitored by measuring the CO_2 concentration in the outlet gas. Once approximately 70 moles of active CaO for CO_2 capture had been obtained, the calcination stage was concluded. N_2 was then fed at a temperature close to 600ºC for 2 hours to accommodate the temperature of the bed for a suitable CASOH operation.

In the CASOH stage example described in this section, a BFG flow rate of 38 Nm³/h was fed, with a composition of approximately 21% CO, 22% CO_2, 7% H_2, and 50% N_2 (see Figure 6.1). A steam flow of 15 Nm³/h was also introduced to maintain an S/CO ratio close to 2 in the feed (see Figure 6.2). Additionally, a nitrogen flow of 38 Nm³/h was fed through the preheaters to ensure safe operation (i.e., to maintain a minimum gas flow while the heaters are operating at high temperatures and also to prevent any flow of combustible gas and steam towards them).

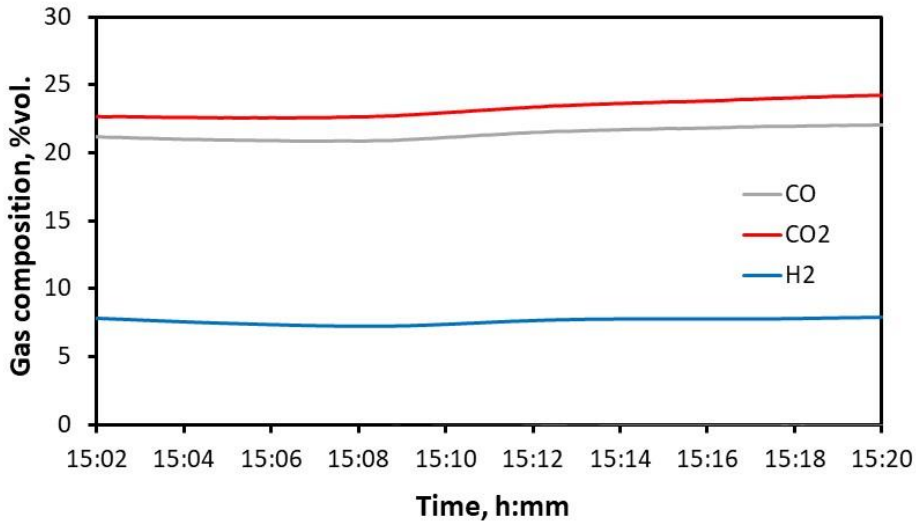

Figure 6.1. Composition of the inlet BFG during the CASOH stage

*This project has received funding from the European Union's Horizon 2020 research and innovation programme under the Grant Agreement No **884418***

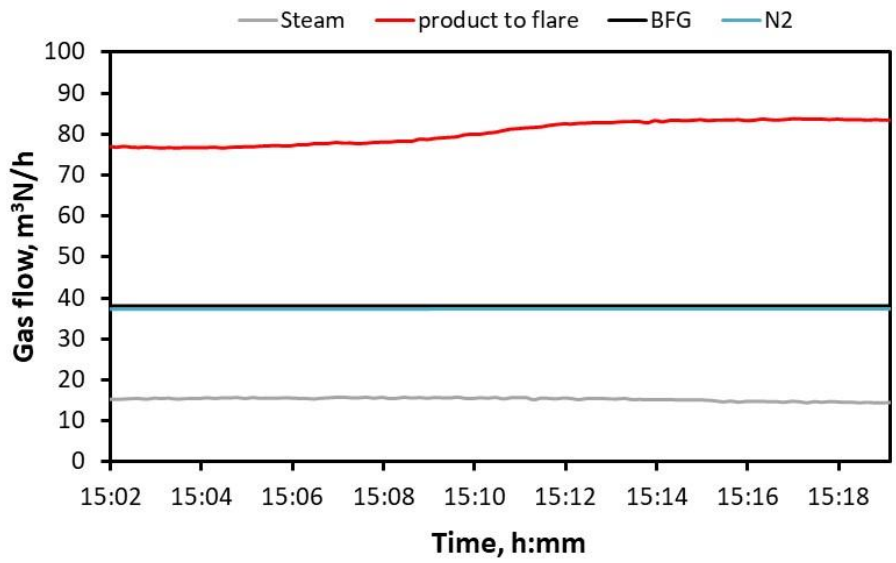

Figure 6.2. Volumetric flowrates (Nm^3/h) of inlet gases (BFG, steam, N_2) and product gas directed to the flare during the CASOH stage

Figure 6.3 shows the temperature of the N_2 across the preheaters (i.e., TH1 and TH2), which maintained a stable value of 725°C, and the temperature of N_2 once it left the preheaters (TH3) and entered the refractory-lined pipe connecting PREH with the reactor, which also remained stable at 590°C during the experiment.

Under these conditions, the total inlet gas flow reached 91 Nm^3/h, resulting in a gas velocity inside the reactor of approximately 0.5 m/s, and consequently, a residence time of about 2 seconds.

*This project has received funding from the European Union's Horizon 2020 research and innovation programme under the Grant Agreement No **884418***

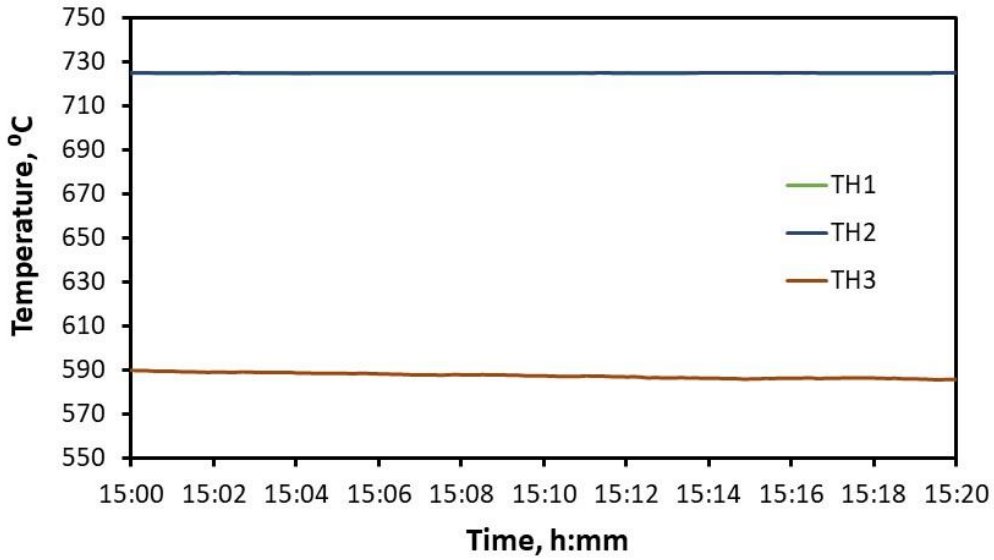

Figure 6.3. Temperature of the inlet N_2 inside (TH1 and TH2) and at the exit (TH3) of the preheaters during the CASOH stage.

Figure 6.4 shows the evolution of the product gas composition obtained during this example of the CASOH stage. As can be seen, during the first 5 minutes (i.e., the pre-breakthrough period), the BFG was almost completely decarbonized and converted into a hydrogen-enriched stream. Under these experimental conditions, the kinetics of the WGS and CaO carbonation reactions were highly favourable, resulting in nearly complete CO conversion and a very high CO_2 capture rate. During this period, CO and CO_2 concentrations in the product gas were less than 1% vol (on a dry basis), indicating a CO_2 capture efficiency of approximately 98%. The removal of CO_2 from the gas phase enhanced H_2 production, resulting in a maximum concentration of 20% vol. (on a dry basis) in the product gas, which aligns with the WGS equilibrium assisted by the simultaneous carbonation of CaO. It is important to note that this product gas would have reached a concentration of 40% vol. of H_2, if the additional N_2 had not been added to ensure the safe operation of the gas preheaters.

After 5 minutes of operation, the carbonation front approached the end of the reacting bed, leading to a progressive decrease in H_2 concentration and an increase in CO and CO_2 concentrations. After just over 10 minutes of operation, the CO_2 sorbent was nearly fully carbonated and stopped capturing CO_2. From that point onwards, the fixed bed acted as a conventional WGS reactor, producing a gas with approximately 11% vol. H_2, 5% vol. CO, and 20% vol. CO_2 in nitrogen.

*This project has received funding from the European Union's Horizon 2020 research and innovation programme under the Grant Agreement No **884418***

The transition from the effective CASOH period to the WGS-only reaction period is also evident in the measurements of the outlet gas flowrate to the flare (gas out in Figure 6.2). The gas flow rate increased from approximately 77 Nm³/h (after steam removal in the drop separator) to about 84 Nm³/h. This increase is attributed to the reduced formation of H_2 and the complete emission of the CO_2 resulting from the WGS reaction.

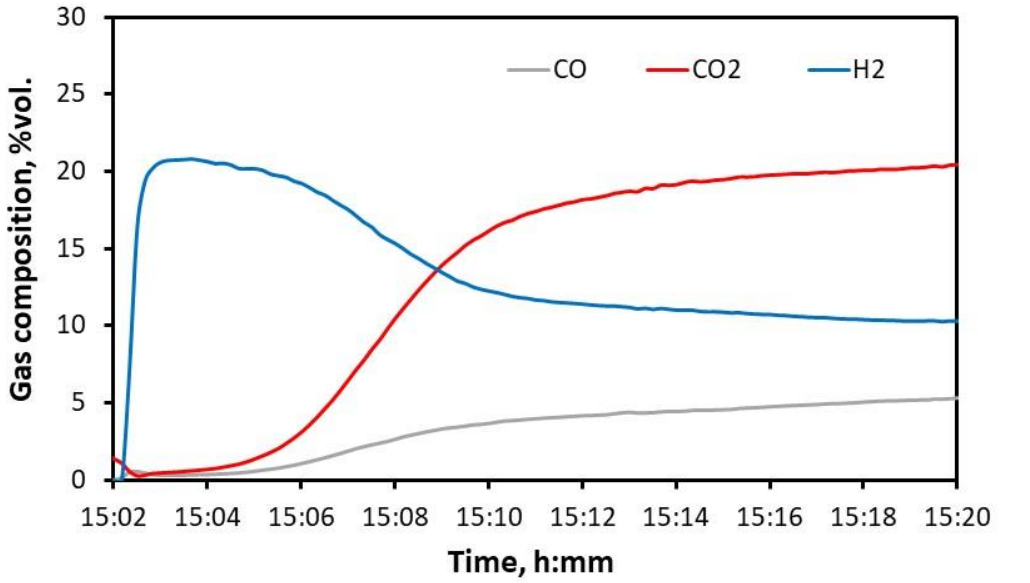

Figure 6.4. Evolution of the composition of the product gas during the CASOH stage.

Figure 6.5 shows the temperature evolution at different points in the reactor during the CASOH stage. Thermocouples TRi specifically indicate the heating in the reactive bed in the second half of the fixed-bed reactor. When half of the CASOH stage had elapsed, the thermocouple located at a height of 0.5 m began to register a rapid temperature increase due to the heat generated by the exothermic WGS and CaO carbonation reactions. As the CASOH stage progressed, the temperature at this point in the reactor rose to a maximum value of approximately 780°C. Since the carbonation front advanced more quickly than the heat exchange front, the carbonated material was left behind at the maximum temperature. Consequently, the temperature at TR_0.5m remained close to 780°C throughout the entire CASOH stage. Meanwhile, thermocouples positioned higher in the solids bed (i.e., TR_0.6m and TR_0.65m) gradually increased their temperature as they were reached by the carbonation front, exhibiting a temperature evolution similar to that observed at TR_0.5m.

*This project has received funding from the European Union's Horizon 2020 research and innovation programme under the Grant Agreement No **884418***

As the carbonation front advanced rapidly, leaving behind the heat released by the reaction, the product gas was only slightly heated during the CO_2 capture period (i.e., between 15:02 and 15:08) and exited at temperatures close to the initial values in the bed. T_{gout} in Figure 6.5 is positioned at the top of the reactor, where no solids are present, and remained stable at around 515ºC during this period. Only when the carbonation front reached the end of the bed, the temperature at T_{gout} started to rise significantly, eventually reaching over 570ºC by the end of the stage.

However, the evolution of the temperature (T_inert) in the fraction of the bed with alumina (at the reactor inlet) differed during the CASOH stage. Initially, this part of the inert bed was at around 570ºC due to the previous temperature conditioning with preheated N_2. However, once the reaction stage started and predominantly cold gases were introduced into the reactor (since both BFG and steam could not be preheated in PREH), the temperature in the inert bed gradually decreased, falling below 300ºC by the end of the CASOH stage.

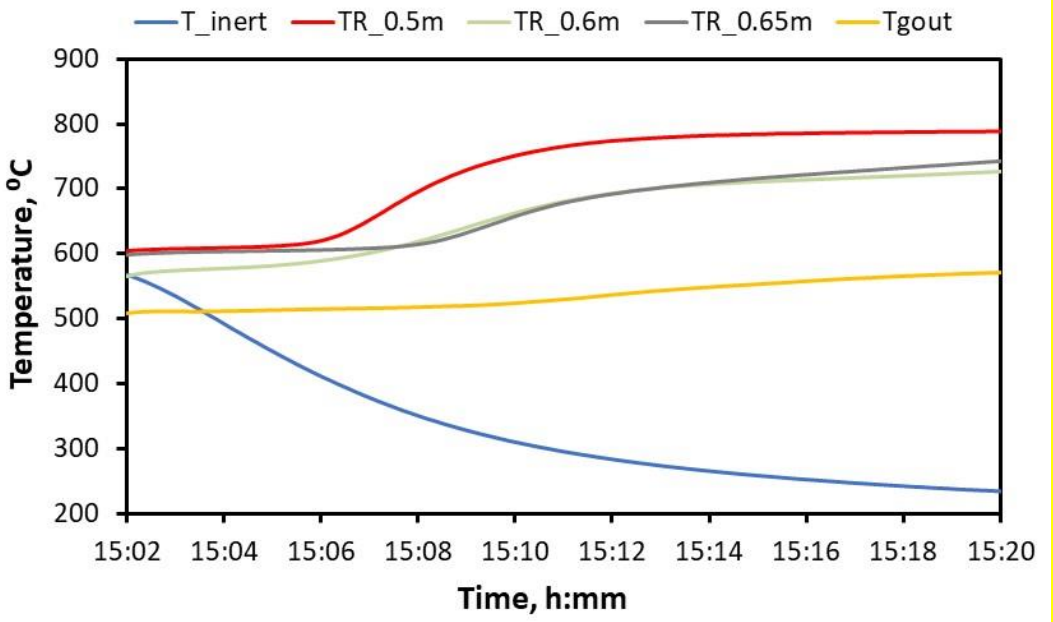

Figure 6.5. Evolution of the temperature profiles at different points of the packed-bed reactor during the CASOH stage.

Regarding pressure (see Figure 6.6), the values showed in P1 (pressure drop in the gas line from the preheaters to the flare) and P_diff (pressure drop across the solid bed) remained stable at 0.32-0.34 bar and 0.03 bar, respectively. It is important to note that the P_diff value aligns with

*This project has received funding from the European Union's Horizon 2020 research and innovation programme under the Grant Agreement No **884418***

the calculation using the Ergun equation for the experimental conditions used example of the CASOH stage.

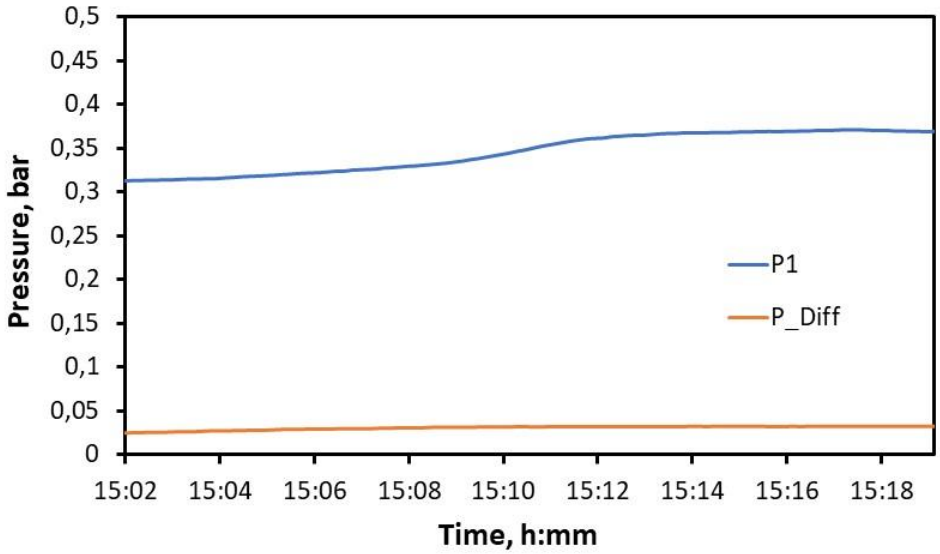

Figure 6.6. Evolution of the pressure drop in the gas line from the preheaters to the flare (P1) and the pressure drop along the packed bed (P_diff) during the CASOH stage.

6.2 Example of a Cu oxidation stage

This section describes an example of a copper oxidation stage using air. This stage is preceded by a CASOH stage and a brief 5-minute purge with nitrogen to remove any residual fuel gas from the pilot plant lines. As a result, at the start of this stage, the copper material is in its metallic form (Cu), and the calcium material is fully carbonated.

In this oxidation stage example, a flow of 52 Nm^3/h of air was introduced, along with an additional 54 Nm^3/h of N_2. This resulted in an inlet gas stream of 106 Nm^3/h with an oxygen concentration of 12% vol. (see Figure 6.7). Under these conditions, the maximum gas velocity within the reactor reached 0.6 m/s, leading to a residence time of approximately 1.67 seconds, which are expected conditions of a CASOH process reactor at industrial scale.

*This project has received funding from the European Union's Horizon 2020 research and innovation programme under the Grant Agreement No **884418***

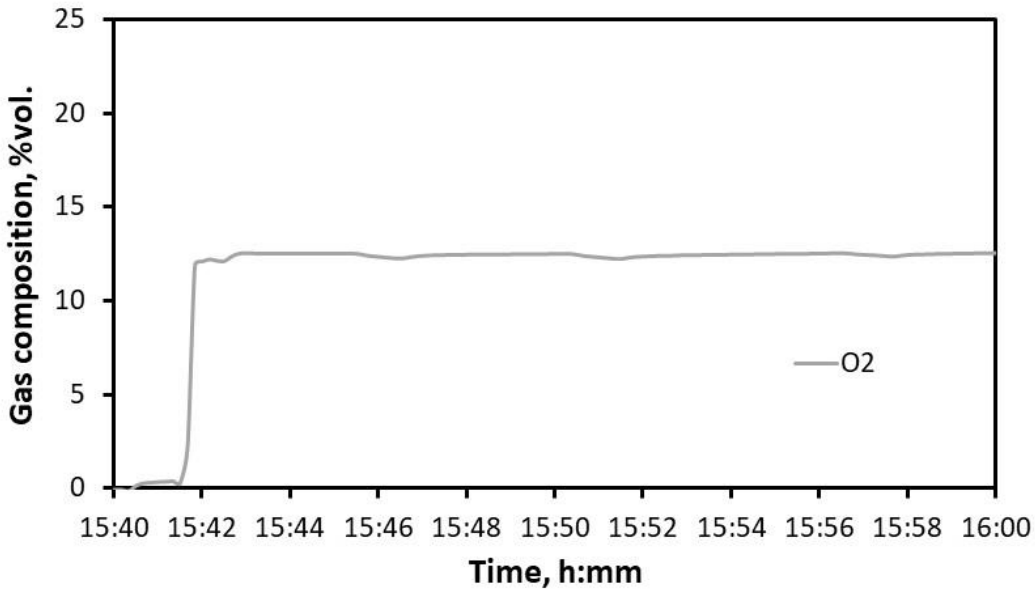

Figure 6.7. Composition of the inlet gas during the oxidation stage

As non-fuel gases were fed and produced during this stage, the gas outlet to the flare was closed, and vent 2 was opened (see PFD in Figure 5.1). Consequently, the flow meter reading on the pipe connected to the flare (FT-500) registered 0 (see Figure 6.8).

*This project has received funding from the European Union's Horizon 2020 research and innovation programme under the Grant Agreement No **884418***

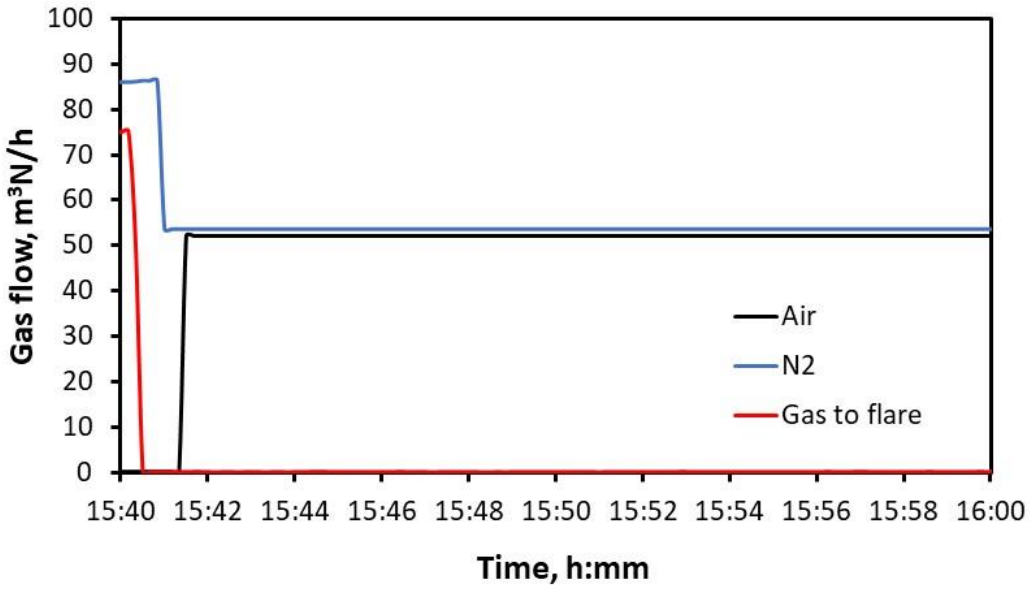

Figure 6.8. Volumetric flowrates (Nm^3/h) of inlet gases (air, N_2) and product gas directed to the flare during the oxidation stage

Figure 6.9 shows the gas temperature across the preheaters (i.e., TH1 and TH2), which maintained a stable value of 725ºC (after a brief initial period of instability due to changes in the inlet flows), and the temperature of the gas at the entrance of the refractory-lined pipe connecting PREH with the reactor (TH3), which was around 640ºC during the experiment.

*This project has received funding from the European Union's Horizon 2020 research and innovation programme under the Grant Agreement No **884418***

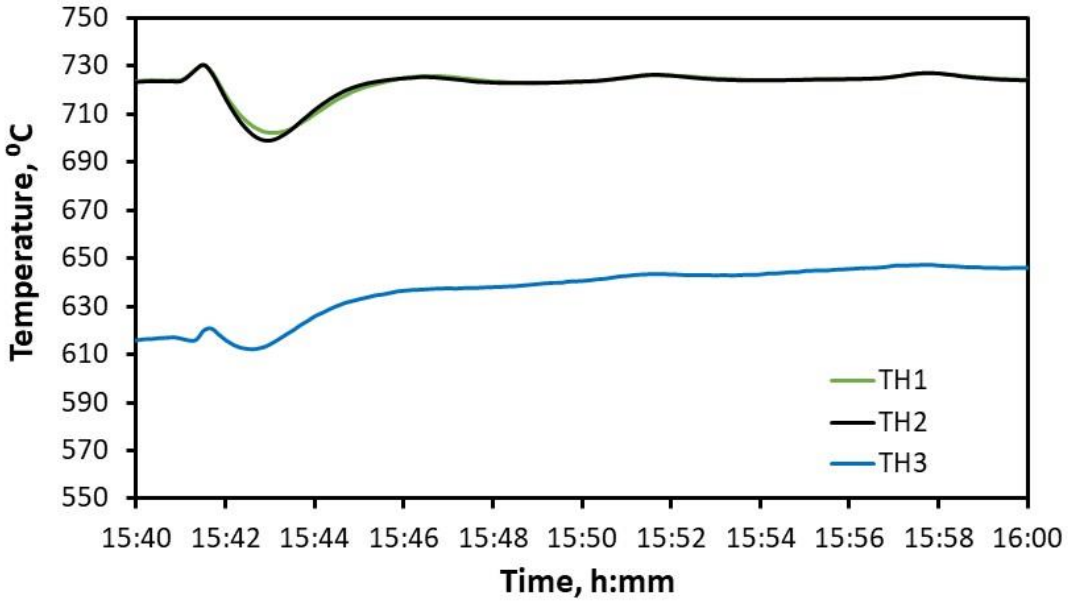

Figure 6.9. Temperature of the inlet air/N_2 inside (TH1 and TH2) and at the exit (TH3) of the preheaters during the oxidation stage.

Figure 6.10 shows the composition of the reactor's exit gas during this stage. As can be seen, during the first 8 minutes of operation (i.e., between 15:41 and 15:53), the oxygen in the inlet gas was almost entirely converted, with O_2 concentrations recorded lower than 0.5% vol. These data demonstrate the extremely rapid kinetics of Cu oxidation even with such low gas residence times. After this period, as the oxidation front approached the end of the bed, the O_2 concentration at the exit gas began to rise rapidly, reaching the inlet value (i.e. 12% vol.) in only 3 minutes (breakthrough period). This sharp oxidation profile further highlights the excellent reactivity of the copper material with oxygen.

Additionally, the temperature increase caused by the heat generated during the oxidation reaction led to the partial calcination of the $CaCO_3$ present in the bed. As shown in Figure 6.10, CO_2 concentrations in the product gas were below 2% at the beginning of the stage, when the bed had not yet reached temperatures high enough to cause significant calcination. However, after 7-8 minutes of operation, there was a substantial increase in CO_2 concentration, reaching up to 10% vol. in the product gas. Based on the monitored CO_2 concentration during this stage, it is estimated that nearly 60 moles of the $CaCO_3$ initially present in the reactor were calcined. The level of calcination is calculated by integrating over time (s) the product of the CO_2

*This project has received funding from the European Union's Horizon 2020 research and innovation programme under the Grant Agreement No **884418***

concentration (mol/Nm^3) measured by the analyzer at the exit of the reactor multiplied by the flow rate of gases measured at the exit (in Nm^3/s). This represents a significant loss of CO_2 during this stage, which could be avoided if the process were conducted at higher pressure, as theoretically designed for the CASOH process at an industrial scale. Moreover, an adequate heat management of the bed, with proper cooling and heating stages using gas recycles before oxidation, can minimize CO_2 slip to values below 1%vol. during Cu oxidation (21). Once a stable O_2 concentration was reached in the product gas (i.e., 12% vol., equal to the inlet gas), all the copper in the bed had been oxidized, and the stage was completed.

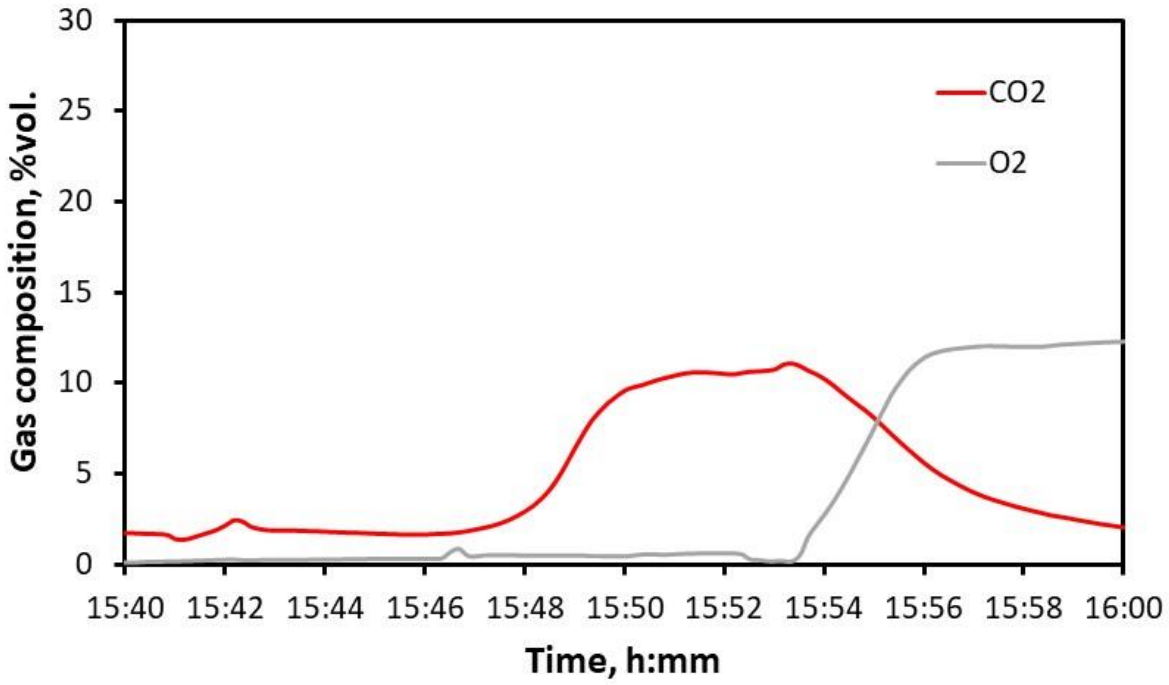

Figure 6.10. Evolution of the composition of the product gas during the oxidation stage.

Figure 6.11 shows the temperature profiles at different points in the reactor during the oxidation stage. As can be seen, the thermocouples inserted into the reactive bed (TRi) indicate that at the start of the stage, the reactive solids were at a temperature between 735 and 760ºC, as a result of the previous CASOH and N_2 purge stages. As oxidation progresses in a very narrow front, as shown in Figure 6.10, the TR_0.5m thermocouple does not detect any significant temperature changes until halfway through the stage (i.e. at 15:48 h). At that moment, a drastic temperature increase was observed, and within approximately 1 minute, this thermocouple

*This project has received funding from the European Union's Horizon 2020 research and innovation programme under the Grant Agreement No **884418***

reached a maximum value of 871ºC. In other words, it experienced a temperature rise of approximately 110ºC due to the heat released during the oxidation of Cu. As the stage progressed, the other downstream thermocouples experienced similar heating. Given the low Cu content in the bed (15% w. CuO diluted in the bed by half due to the presence of calcium material), the oxidation front advances very quickly, and the heat generated accumulates in the converted solids. Therefore, despite the large amount of heat generated in this stage, the exit gas temperature (Tgout) barely increased during the operation. Only when the oxidation front approached the end of the bed (i.e. at 15:52 h), the temperature at Tgout began to rise slightly, eventually reaching over 658ºC by the end of the stage.

Regarding the temperature of the alumina bed at the bottom of the reactor (T_inert), its value gradually increased during this stage. It started at values close to 300ºC, as low-temperature BFG and steam had been fed during the previous CASOH stage. However, the preheated air/N_2 feed caused the temperature of the inert material to rise, reaching nearly 575ºC by the end of the oxidation.

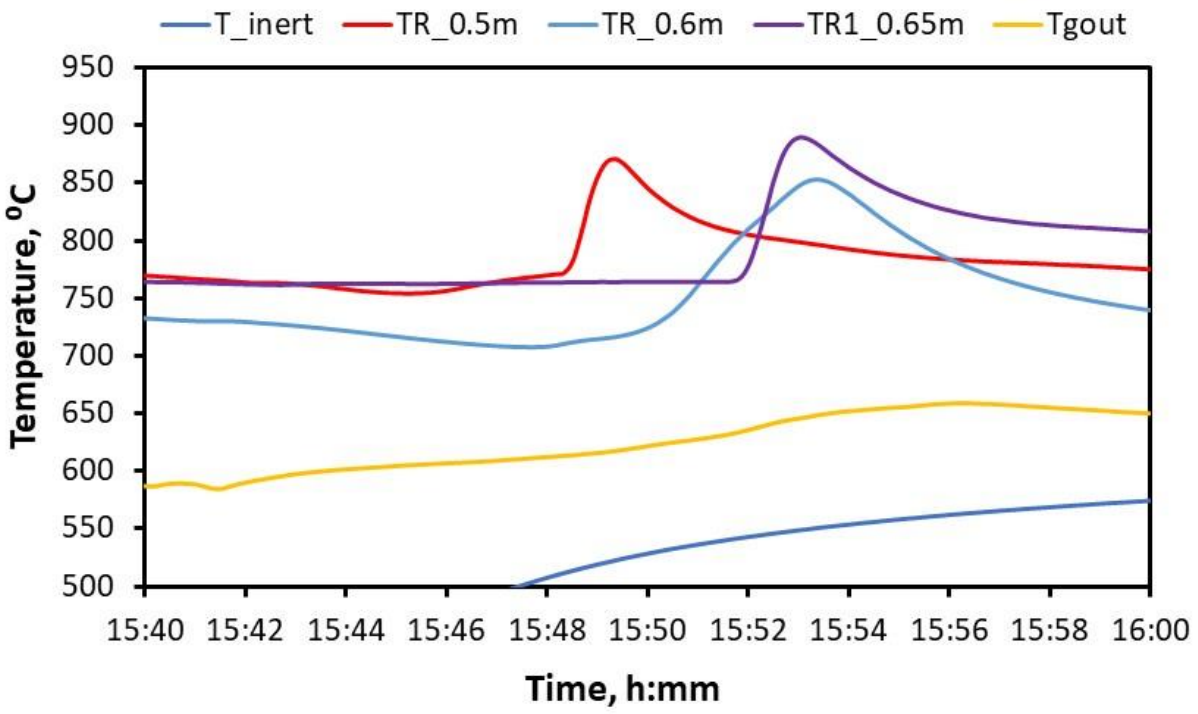

Figure 6.11. Evolution of the temperature profiles at different points of the packed-bed reactor during the oxidation stage

*This project has received funding from the European Union's Horizon 2020 research and innovation programme under the Grant Agreement No **884418***

As for the pressure (see Figure 6.12), the value recorded at P1 suddenly dropped from 0.33 to 0.15 bar when the product gas outlet was switched from the flare to vent 2, indicating the significant pressure drop imposed by the flare of the pilot plant. This unusual pressure drop problem was corrected in subsequent test by cleaning the filter acting as flame extinguisher located before the torch. Regarding the pressure drop recorded across the solid bed (P_diff), the values remained below 0.05 bar throughout the experiment, which is consistent with the theoretical calculation using the Ergun equation for the conditions of this test

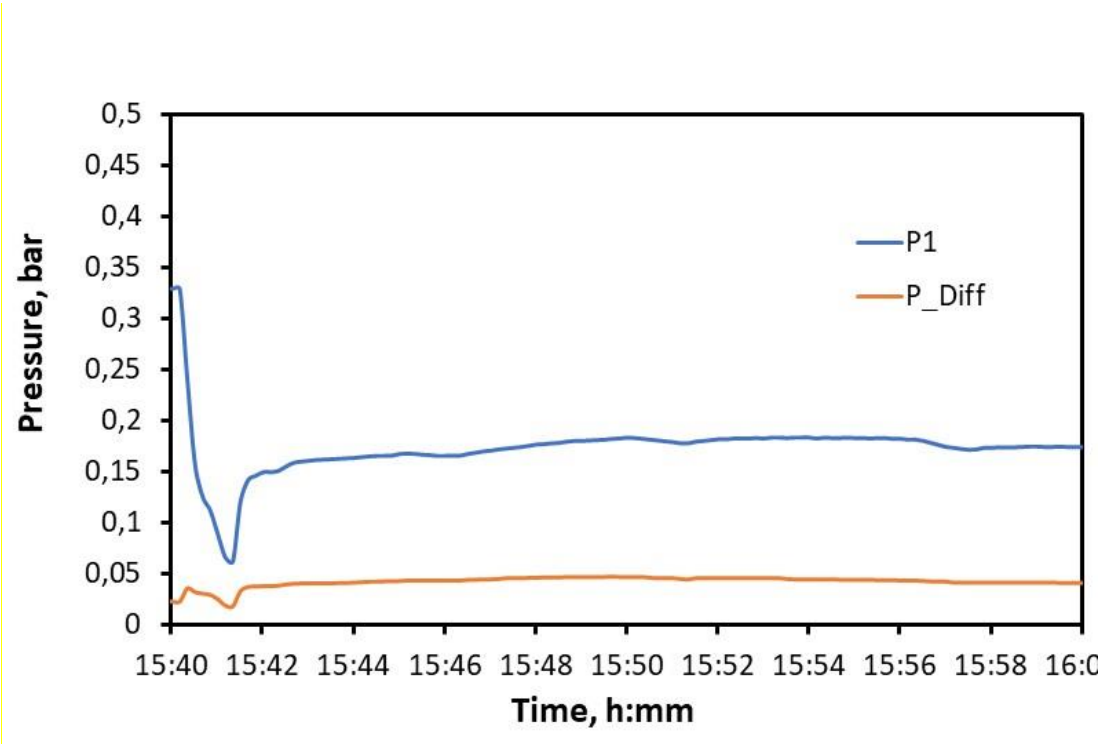

Figure 6.12. Evolution of the pressure drop in the gas line from the preheaters to vent 2 (P1) and the pressure drop along the packed bed (P_diff) during the oxidation stage

*This project has received funding from the European Union's Horizon 2020 research and innovation programme under the Grant Agreement No **884418***

6.3 Example of a CuO reduction before/or during calcination of $CaCO_3$

This example of CuO reduction stage with BFG was preceded by a preheating period using air and N_2, followed by a final purge with only N_2 to remove any traces of oxygen from the pilot plant lines. During the preheating period, the temperatures in the preheaters (TH1 and TH2) were maintained at 700 °C, resulting in a gas outlet temperature from the preheaters of approximately 600 °C. As a result of that, a temperature close to 600 °C was achieved to initiate the reduction of CuO with BFG.

Some minutes before the reaction stage began, a flow of 46 Nm^3/h of BFG was directed exclusively to the torch. Simultaneously, a flow of 68 Nm^3/h of N_2 was supplied through the preheaters to ensure safe operation. This resulted in a total flow of 114 Nm^3/h to the torch, as shown in Figure 6.13. Just before starting the CuO reduction with BFG, the N_2 flow was reduced to 52 Nm^3/h. Both BFG and N_2 inlet flows were then kept constant throughout the entire CuO reduction stage.

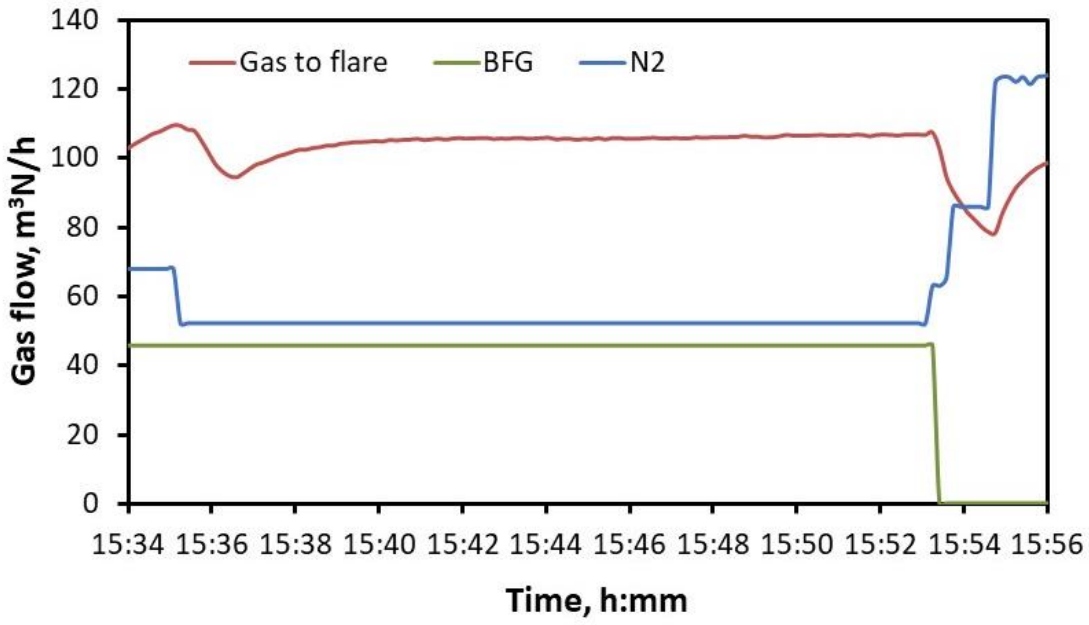

Figure 6.13. Volumetric flowrates (Nm^3/h) of inlet gases (BFG, N_2) and product gas directed to the flare during the CuO reduction stage.

*This project has received funding from the European Union's Horizon 2020 research and innovation programme under the Grant Agreement No **884418***

Figure 6.14 shows the temperature of the N_2 passing through the preheaters (TR1 and TR2), which remained very stable at around 700 °C during operation (except for a brief transition period when the N_2 flow was reduced from 68 to 52 Nm³/h, causing a slight temperature increase to nearly 710 °C). As a result of this preheating, the N_2 finally fed into the reactor maintained a temperature (TH3) between 590 and 600 °C.

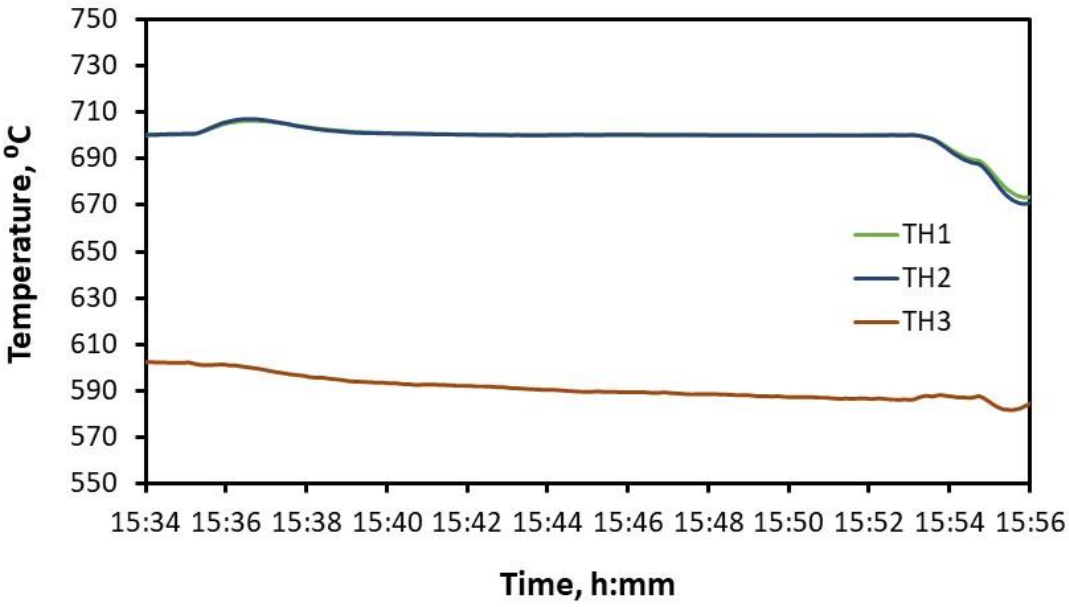

Figure 6.14. Temperature of the inlet N_2 inside (TH1 and TH2) and at the exit (TH3) of the preheaters during the CuO reduction stage.

At 15:36 (h:mm), a flow of 46 Nm³/h of BFG was introduced into the reactor (mixed with 52 Nm³/h of preheated N_2) with a composition of 20% CO, 23% CO_2, 6% H_2, and 51% N_2 (see the signal from analyzer 1 in Figure 6.15). Under these operating conditions, the gas reached a maximum velocity in the reactor of nearly 0.55 m/s, resulting in a residence time within the reactor of approximately 1.8 seconds.

*This project has received funding from the European Union's Horizon 2020 research and innovation programme under the Grant Agreement No **884418***

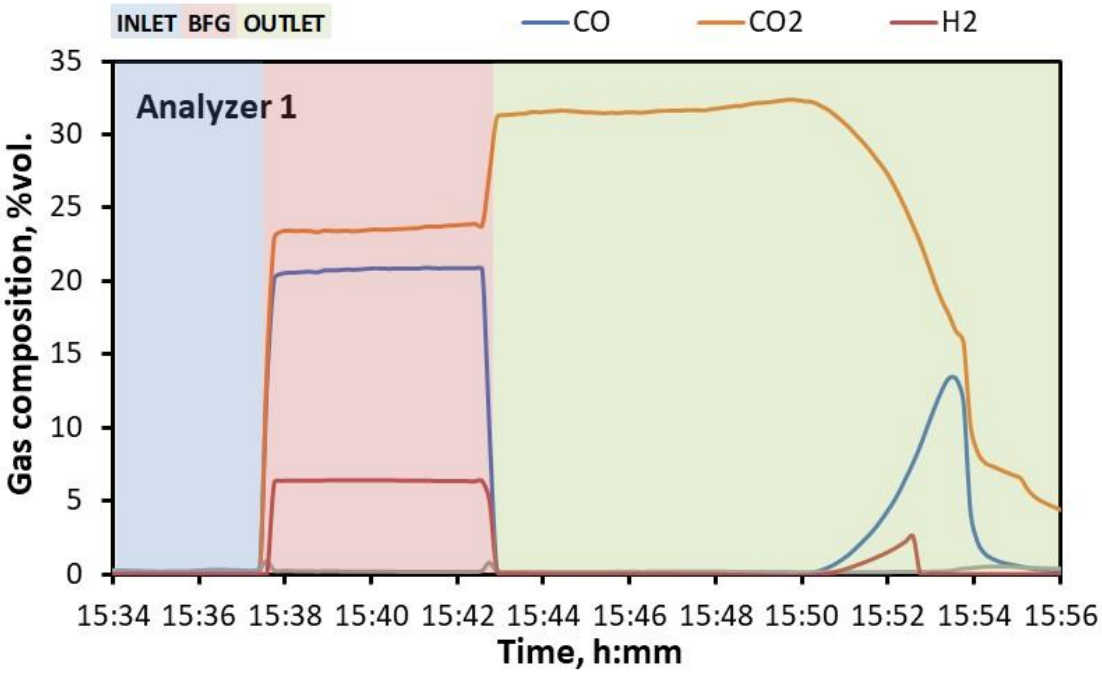

Figure 6.15. Evolution of the composition of BFG and the product gas measured by Analyzer 1 during the CuO reduction stage. Note the colour codes changes in the graph, as noted at the top of the Figure, indicating that the gas sampling was changed to different positions in the pilot, to ensure consistency of measurements between Analyzer 1 and 2.

Figure 6.16 shows the concentration at the reactor exit during the first minutes of the stage (signal from analyzer 2). A dramatic increase in CO_2 concentration in the product gas can be observed, reaching values close to 30% vol. on a dry basis. Regarding the fuel gases in the incoming BFG, there was an almost complete conversion of H_2 and CO, with both gases registering less than 0.2% vol. on a dry basis in the outlet gas.

*This project has received funding from the European Union's Horizon 2020 research and innovation programme under the Grant Agreement No **884418***

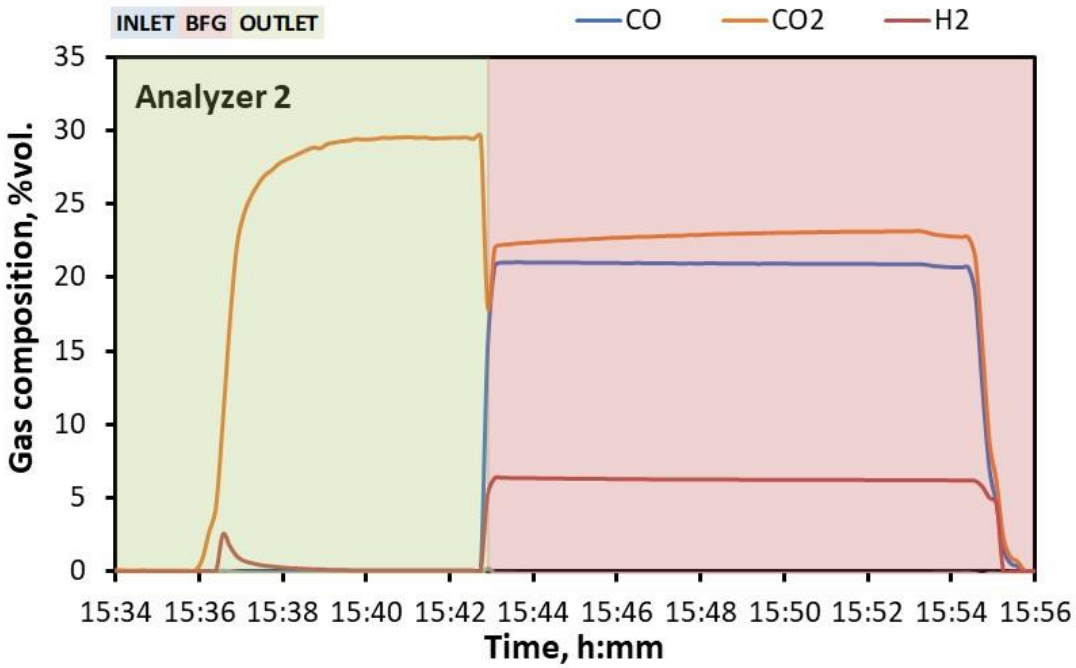

Figure 6.16. Evolution of the composition of BFG and the product gas measured by Analyzer 2 during the CuO reduction stage.

Once half of the stage had elapsed (around 15:43), the measurements from the two analyzers in the pilot plant were swapped. Analyzer 1 (Figure 6.15) began measuring the composition of the product gas, while analyzer 2 recorded the composition of the incoming BFG. This change was made to verify that the measurements from both analyzers were consistent. As expected, analyzer 2 measured the same BFG composition at the inlet throughout the entire reduction stage. On the other hand, analyzer 1 continued to measure CO_2 concentrations in the product gas close to 30%, with barely any unconverted CO and H_2 detected.

The concentration of CO_2 in the product gas, along with the measured gas flowrate in the line leading to the torch, indicate that a partial calcination of $CaCO_3$ also occurred in addition to the reduction of CuO-based solids by the oxidation of CO and H_2 present in the BFG. Based on the dilution of BFG with N_2 in the feed, the CO_2 concentration in the product gas was expected to be around 20% vol., but it was actually 30% vol. throughout the pre-breakthrough period. Moreover, considering the inlet flow rate and excluding the H_2 oxidized to H_2O (and thus retained in the drop separator), the expected total outlet flow to the torch should have been about 95 Nm^3/h, yet an actual flow of approximately 105 Nm^3/h was measured during the experiment (see Figure 6.13). This excess of 10 Nm^3/h in the product gas confirmed that the reduction of

*This project has received funding from the European Union's Horizon 2020 research and innovation programme under the Grant Agreement No **884418***

CuO with BFG occurred, together with a simultaneous partial calcination of $CaCO_3$, as considered in the classical regeneration stage of the CAOH process.

After extending the operation for 5 minutes, a significant increase in CO and H_2 concentrations (and a decrease in CO_2) was observed in the outlet gas. This indicated that the CuO reduction front was reaching the end of the reacting solids bed. After two minutes of observing a very rapid breakthrough curve in the outlet gas, the CuO reduction stage was concluded at 15:53. At this point, the composition of the product gas was similar to the inlet gas (considering the N_2 dilution). Based on the excess CO_2 and the flow rate observed throughout the pre-breakthrough period, it was estimated that approximately 120 moles of $CaCO_3$ were calcined during this CuO reduction stage. Figure 6.17 illustrates the temperature evolution at various points in the reactor during the CuO reduction stage. The initial temperature profile of the bed was around 600 °C. As observed in previous stages, during the first half of the stage, the temperature measured by thermocouples located in the latter half of the bed remained constant. This indicates that the reduction front advanced ahead of the heat exchange front, so all the heat generated from the reduction of CuO to Cu remained in the solids behind the reaction front.

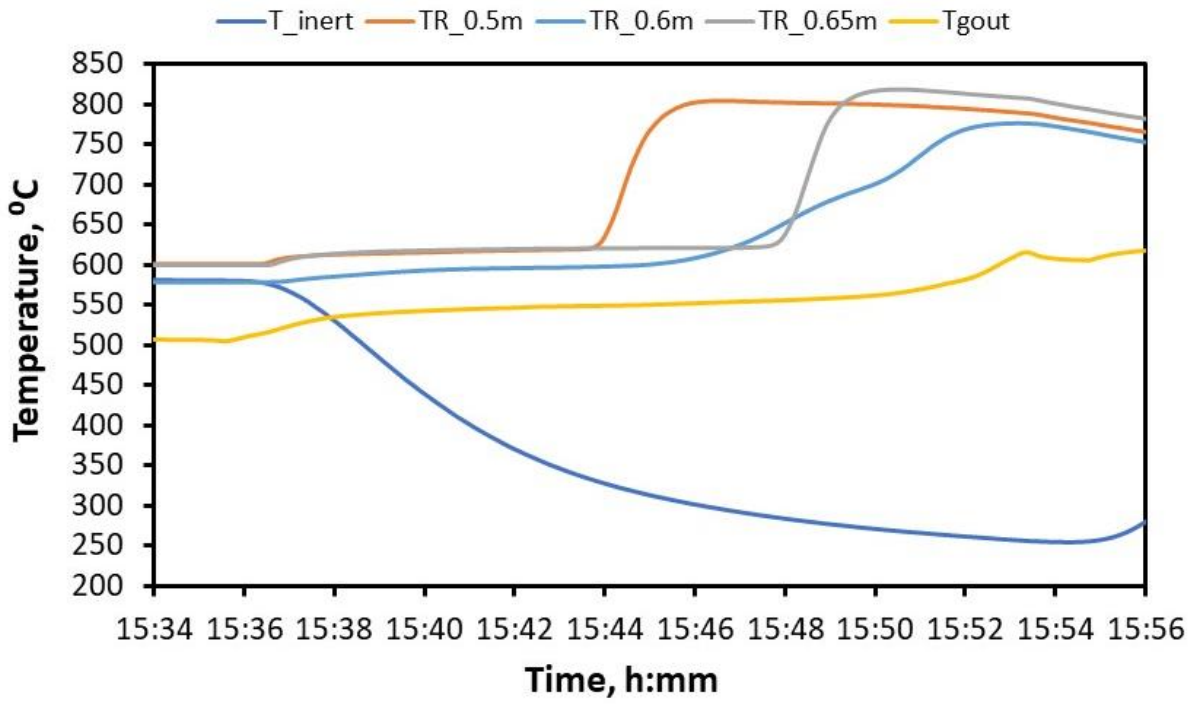

Figure 6.17. Evolution of the temperature profiles at different points of the packed-bed reactor during the CuO reduction stage

*This project has received funding from the European Union's Horizon 2020 research and innovation programme under the Grant Agreement No **884418***

After 8 minutes of operation (exactly half of the total duration of the stage), the thermocouple positioned at the middle of the bed (TR_0.5 m) experienced a sudden temperature increase as it was reached by the reduction front. This sharp temperature rise confirms the rapid kinetics of CuO reduction with CO and H2 present in the BFG. Thermocouples located further along the bed showed a similar trend, reaching a maximum temperature of up to 820 ºC at TR_0.65 m. As seen in other stages, once the reaction front moved through a section of the reactor, the converted solids stabilized at this maximum temperature, creating a heat plateau.

A different trend was observed in the lower section of the reactor, occupied by inert alumina. As with CASOH stages, the temperature (T_inert) gradually decreased as the BFG+N_2 gas mixture was fed in, since the BFG was supplied directly without preheating.

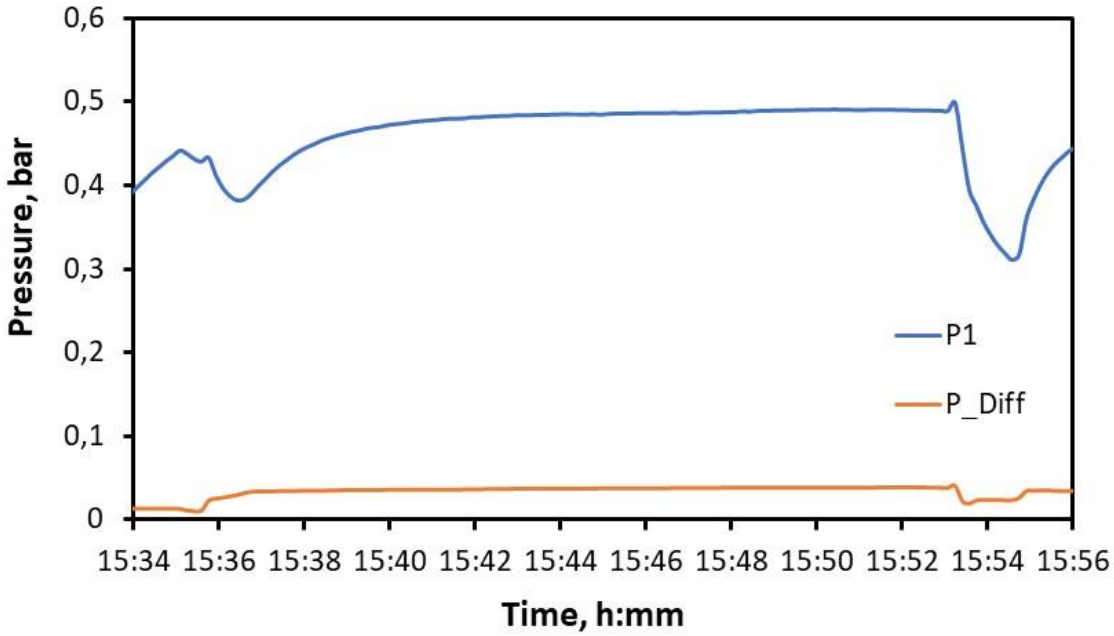

Figure 6.18. Evolution of the pressure drop in the gas line from the preheaters to the flare (P1) and the pressure drop along the packed bed (P_diff) during the CuO reduction stage

Regarding the pressure (see Figure 6.18), P1 (pressure drop in the gas line from the preheaters to the flare) showed a slight fluctuation at the start of the stage but then remained stable at

*This project has received funding from the European Union's Horizon 2020 research and innovation programme under the Grant Agreement No **884418***

around 0.48 bar throughout the CuO reduction. The pressure drop across the bed (P_diff) followed a similar trend, remaining close to 0.03 bar.

6.4 Heat removal/supply stages

As outlined in the full design of the CASOH process, intermediate stages involving the removal or addition of heat to the solid bed using an inert gas (Nitrogen) are necessary between the main reaction steps (i.e., CASOH, Cu oxidation, CuO reduction, and $CaCO_3$ calcination). This allows for adjusting the bed temperature under different conditions, either for safety reasons (such as starting exothermic gas-solid reactions with a sufficiently cool bed to avoid hot spots) or to ensure that the bed is at the high temperatures required for the solids to be chemically active (approximately T>350ºC for Cu-based materials and T>550ºC for Ca-based materials).

Additionally, at an industrial scale, the CASOH process is expected to use internal N_2 recirculation for heat removal. For this purpose, the necessary equipment was acquired for the TRL7 pilot plant (including a nitrogen blower, as detailed in Deliverable D2.2), and gas lines were designed and installed to carry out these N_2 recirculations. However, as also described in D2.2, AM R&D supplies a large external line (up to 200 Nm^3/h) of industrial-grade N_2 to the pilot plant, making so far unnecessary the use of the N_2 gas recycle originally planned for the pilot.

This section describes two examples of heat removal and addition stages in the solids bed. These types of heating/cooling stages have been frequent and time-consuming during the initial dynamic test.

The first example is a heat removal operation following a stage of CuO reduction with simultaneous $CaCO_3$ calcination, which left the bed at temperatures close to 850ºC, which is too high temperature to start a new decarbonization and BFG upgrading stage via a CASOH stage. In this specific case, a flow of approximately 120 Nm^3/h of N_2 was introduced in order to cool down the bed of solids to temperatures around 600 ºC.

As shown in Figure 6.19, the reactor came from a CuO reduction stage carried out feeding around 45 Nm^3/h of BFG mixed with 50 Nm^3/h of N_2. At 15:53 h, the CuO reduction stage finished, and then the supply of steelmaking gas was interrupted, and the N_2 flow increased to 120 Nm_3/h. The heat removal stage lasted for one hour, after which the flowrate of N_2 was reduced again, and the flows of BFG and N_2 was restored in 45 and 50 Nm_3/h, respectively, to initiate a CASOH stage at 16:55 h.

*This project has received funding from the European Union's Horizon 2020 research and innovation programme under the Grant Agreement No **884418***

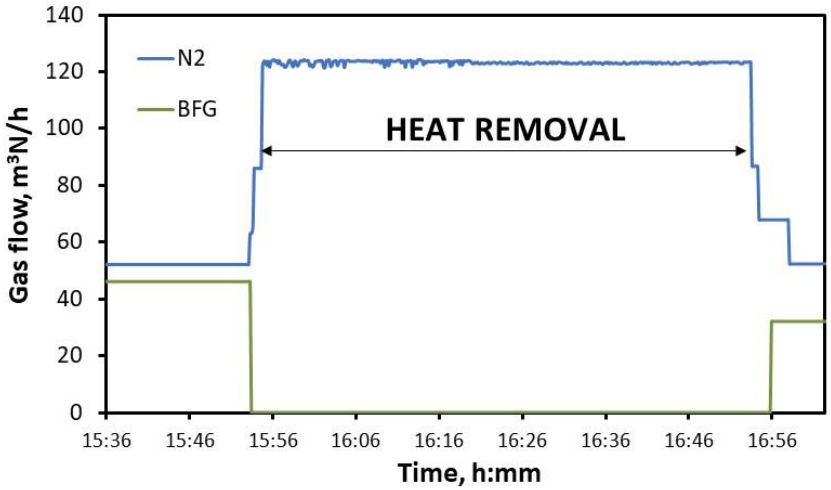

Figure 6.19. Volumetric flowrates (Nm^3/h) of inlet gas during the heat removal stage.

To reduce the reactor temperature to values close to 600 °C, a setpoint of 700 °C was established in the gas preheaters (TH1 and TH2), which resulted in a temperature of the N_2 directed to the reactor (TH3) of approximately 620 °C. As can be seen in Figure 6.20, these values remained stable throughout the entire heat removal stage, except during the transition periods caused by changes in the reactor inlet flows.

*This project has received funding from the European Union's Horizon 2020 research and innovation programme under the Grant Agreement No **884418***

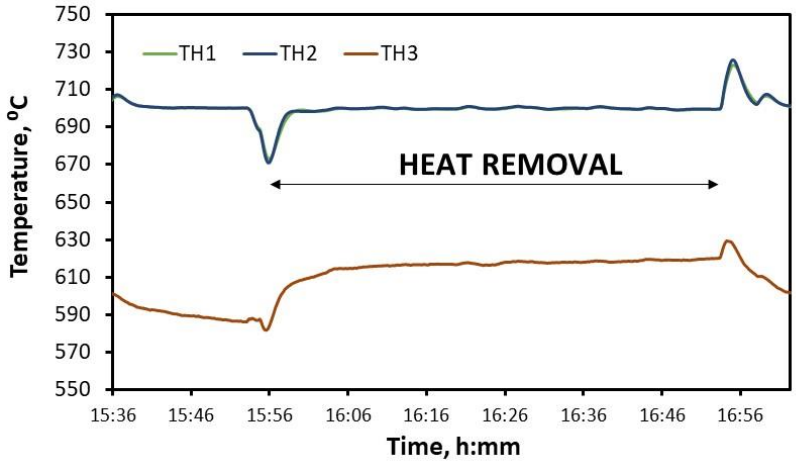

Figure 6.20. Temperature of the inlet N_2 inside (TH1 and TH2) and at the exit (TH3) of the preheaters during the heat removal stage.

Figure 6.21 shows the evolution of the pressure drop in the gas line from the preheaters to the flare (P1) and the pressure drop along the packed bed (P_diff) during the heat removal stage. As can be seen in the figure, the pressure in the N_2 line from the preheaters to the flare (P1) remained relatively stable at values around 0.45 bar, whereas the pressure drop in the reactor was about 0.03 bar along the whole cooling stage.

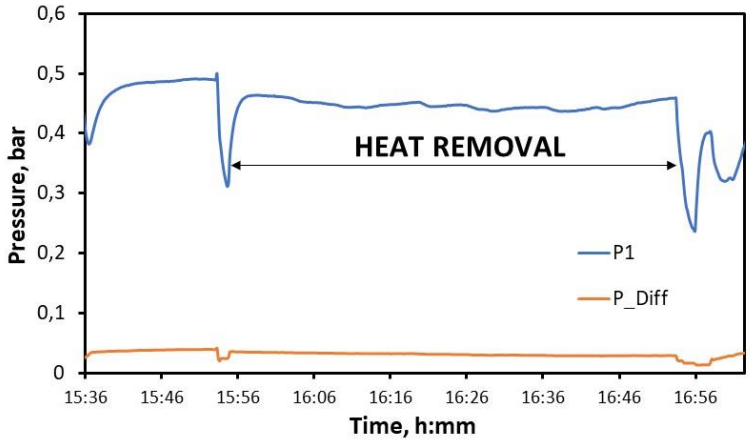

Figure 6.21. Evolution of the pressure drop in the gas line from the preheaters to the flare (P1) and the pressure drop along the packed bed (P_diff) during the heat removal stage.

*This project has received funding from the European Union's Horizon 2020 research and innovation programme under the Grant Agreement No **884418***

Regarding the temperature evolution within the bed, Figure 6.22 shows that immediately after introducing N_2 into the reactor (at 15:53h), the temperatures in the bed (TRi) progressively decreased until they reached values close to 600 ºC by the end of the stage, which were the desired conditions to initiate the subsequent CASOH stage. Moreover, the temperature of the thermocouple located in the inert alumina bed, which started at low values around 250 ºC after the previous CuO reduction stage with BFG, increased during this period to approximately 600 ºC.

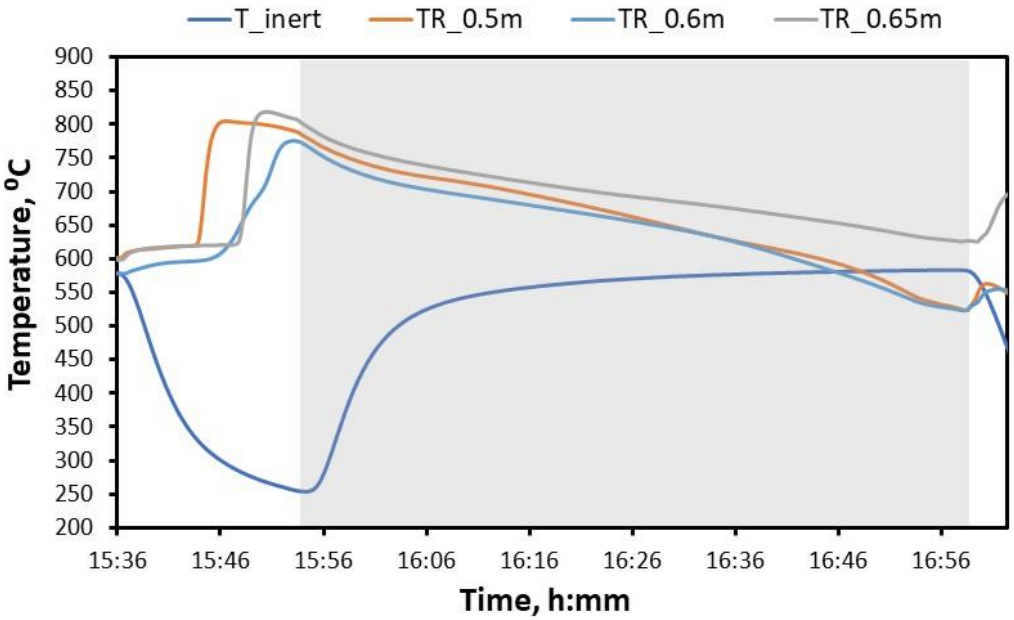

Figure 6.22. Evolution of the temperature profiles at different points of the packed-bed reactor during the heat removal stage.

Figures 6.23 and 6.24 show the measurements recorded by Analyzer 1 and 2, respectively, during the entire heat removal stage. In Figure 6.23, it can be observed that once the supply of BFG to the reactor was cut off, the CO and H_2 concentrations in the outlet gas dropped sharply to zero. The CO_2 concentration also decreased dramatically, though the drop slowed as it approached 5% vol. CO_2. This was due to the high temperatures in the reactor facilitating some degree of calcination upon the introduction of N_2.

*This project has received funding from the European Union's Horizon 2020 research and innovation programme under the Grant Agreement No **884418***

During the first minutes of heat removal, the CO_2 concentration in the outlet gas (see Analyzer 1 reading in Figure 6.23) progressively decreased until it reached 0.5% CO_2. After approximately one-third of the stage, the measurements from both analyzers were switched to verify that the inlet and outlet gas concentrations were being measured correctly. That is, from 16:14h onward, Analyzer 1 measured the inlet gas (100% N_2) and Analyzer 2 measured the reactor outlet gas.

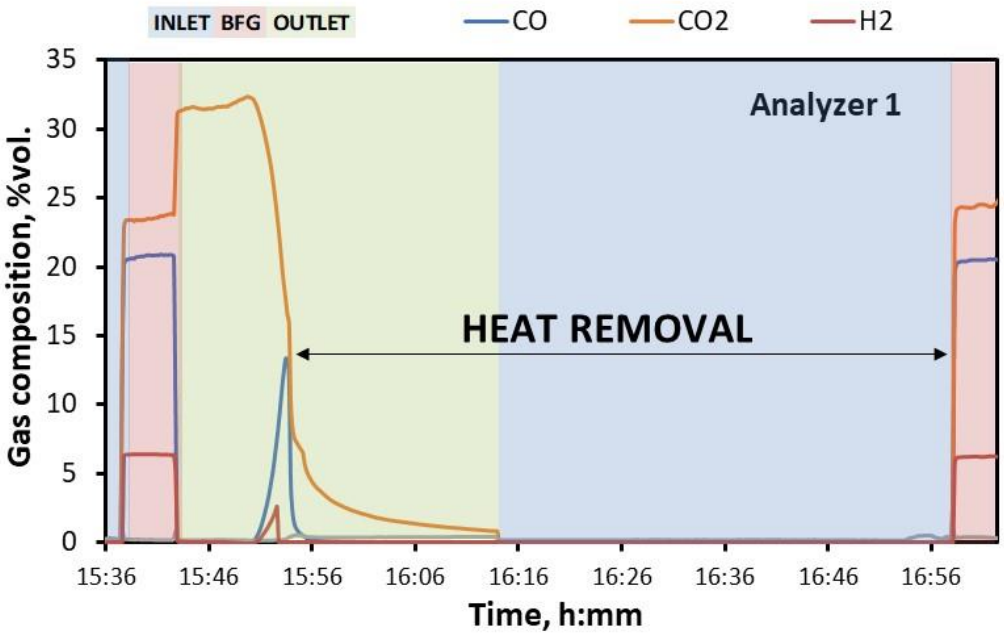

Figure 6.23. Evolution of the composition of inlet/product gas measured by Analyzer 1 during the heat removal stage.

Looking at the concentration of CO_2 measured by Analyzer 2 (see Figure 6.24), the value approached zero after more than half of the stage, since the temperatures in the reactor temperatures at that time (below 700 °C, according to Figure 6.22) were too low for further calcination of $CaCO_3$. Finally, the heat removal stage concluded at 16:58h, after 65 minutes of operation. At that point, a subsequent CASOH stage began (see the rise in CO, CO_2, and H_2 concentrations in the inlet gas measured by Analyzer 1, as shown in Figure 6.23).

*This project has received funding from the European Union's Horizon 2020 research and innovation programme under the Grant Agreement No **884418***

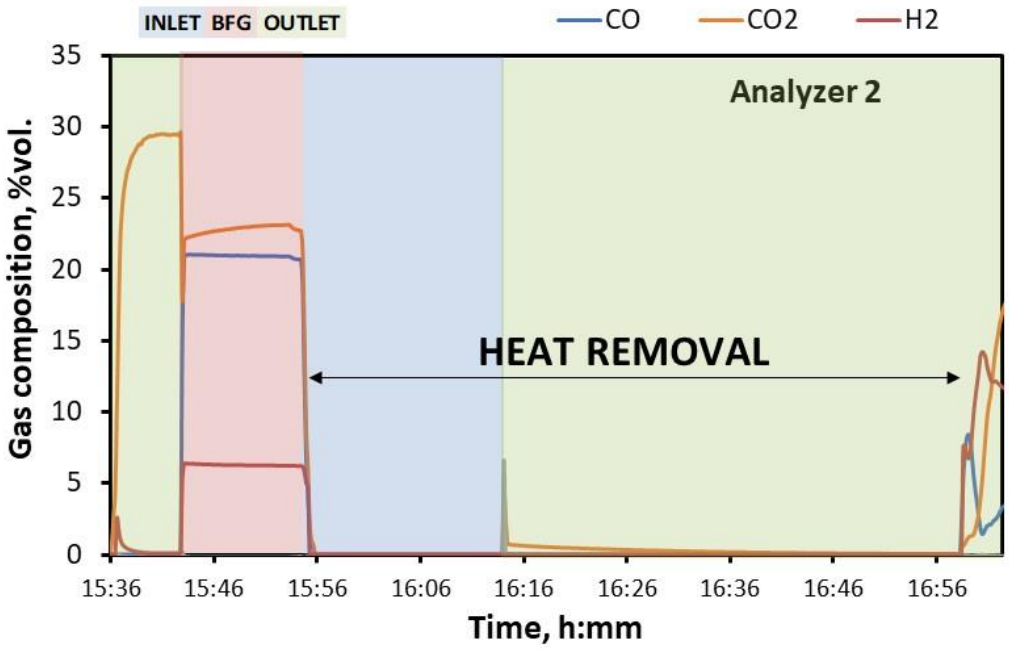

Figure 6.24. Evolution of the composition of inlet/product gas measured by Analyzer 2 during the heat removal stage.

The following paragraphs describe an example of a bed heating stage without a chemical reaction. In this case, the previous day concluded with a CuO reduction stage and simultaneous partial calcination of $CaCO_3$. As a result, the bed contained reduced copper and partially calcined calcium-based material, creating the appropriate conditions for a CASOH stage. Early in the morning, the bed temperature ranged between approximately 400 and 500 °C, making it necessary to heat it to around 600 °C using only N_2 to avoid altering the chemical composition of the copper-based material.

Figure 6.25 shows the flowrates of N_2 used during this heating stage. Initially, low flows of around 50 Nm³/h were used, and after almost an hour of heating, they were progressively increasing until a value of 120 Nm³/h was reached. At certain points, a maximum flow rate of 140 Nm³/h was applied to observe the response of the gas preheaters and also to assess the pressure drop in the system. The bed preheating stage lasted approximately 3.5 hours.

*This project has received funding from the European Union's Horizon 2020 research and innovation programme under the Grant Agreement No **884418***

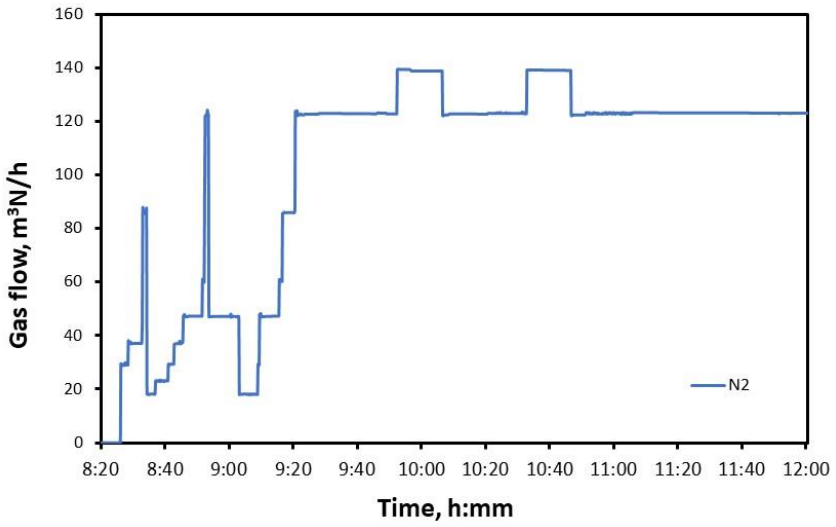

Figure 6.25. Volumetric flowrates (Nm^3/h) of inlet gas during an example of heating period.

Moreover, Figure 6.26 shows the evolution of the setpoint values for the preheaters (TH1 and TH2) throughout the heating process, as well as the resulting temperature of the N_2 ultimately fed into the reactor (TH3). The inlet gas heating curve gradually increased until it reached 600 °C, requiring the temperatures of TH1 and TH2 to be raised to 700 °C.

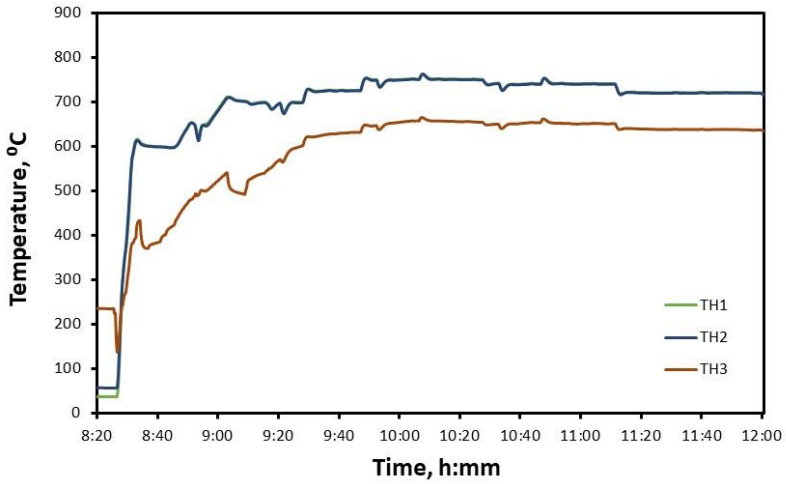

Figure 6.26. Temperature of the inlet N_2 inside (TH1 and TH2) and at the exit (TH3) of the preheaters during an example of heating period.

*This project has received funding from the European Union's Horizon 2020 research and innovation programme under the Grant Agreement No **884418***

On the other hand, Figure 6.27 shows the temperature evolution at various points in the solids bed during this heating stage. After the previous reduction/calcination stage, the bed lost some of the accumulated heat overnight, leaving it initially at temperatures between 400 and 530 ºC. Since the preheaters require a transitional heating phase to reach their operating temperature (in this case, 700 ºC for TH1 and TH2), relatively cold N_2 was introduced into the reactor during the first minutes, which naturally caused a drop in the solids temperature. This cooling propagated through the inert section (T_inert) and the thermocouples located in the reactive zone of the fixed bed (TRi).

The figure illustrates how the initial cooling wave, caused by the preheaters' operation, was followed by a gradual heating as the setpoints for TH1 and TH2 were increased, both evolving as the stage progressed. After 3.5 hours of heating, the reactor temperatures approached an asymptotic level near 600 ºC, marking the end of the heating process and preparing the reactor for the next CASOH stage.

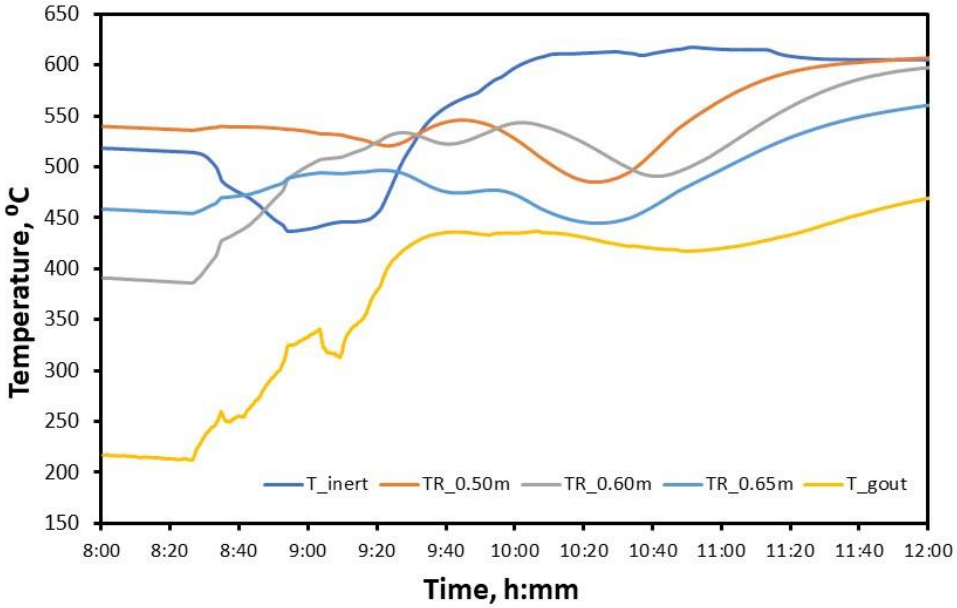

Figure 6.27. Evolution of the temperature profiles at different points of the packed-bed reactor during an example of heating period.

Regarding the pressures (see Figure 6.28), when initially operating with a low N_2 flow rate, the recorded pressure drop from the preheaters to vent 2 (P1) remained around 0.05 bar. During this period, the pressure drop across the solids bed (P_diff) generally stayed below 0.01 bar. As

*This project has received funding from the European Union's Horizon 2020 research and innovation programme under the Grant Agreement No **884418***

expected, with a significant increase in the gas flow rate, the values of P1 and P_diff rose, reaching maximum levels of 0.25 and 0.04 bar, respectively.

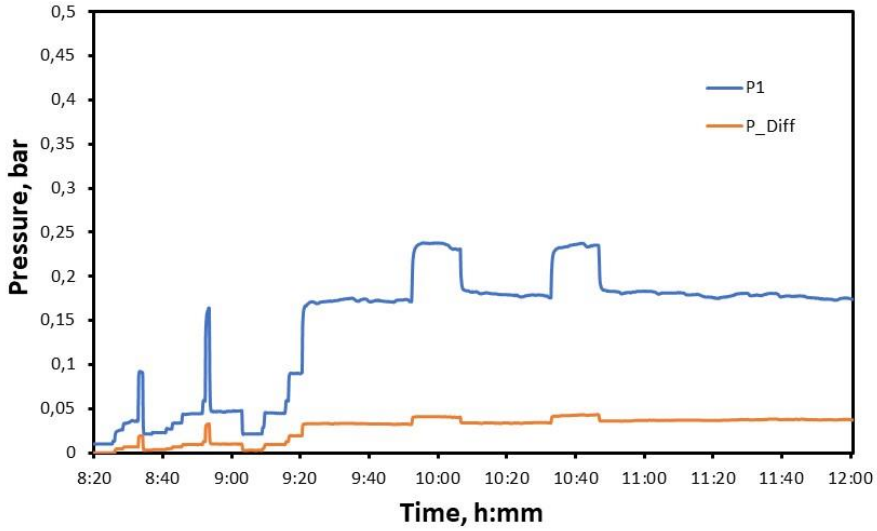

Figure 6.28. Evolution of the pressure drop in the gas line from the preheaters to Vent 2 and the pressure drop along the packed bed (P_diff) during an example of heating period.

7. Tuning reactor model to TRL7 results

As mentioned above, a reactor model able to simulate all reaction stages taking place in a full CASOH loop, including heating/cooling operations of the bed, is a valuable tool for the interpretation of experimental results from the TRL7 pilot, and for the scale up of these results. CSIC has developed such a model and has already demonstrated its capability to fit data from low TRL reactor experiments [5]. The model has been adapted and fitted to the available information from the data at TRL7 reported in section 6 and Annex 10.2 is given below. The final version of the model will be available when the long duration experiments have been carried out. However, the adequate comparison of the model with experimental data, as noted in section 6, by introducing reasonable changes in the fitting parameters at a particle level noted below, allows us to claim that the tuned model resulting from the experimental validation from dynamic test described above is already useful for the final CASOH plant design exercises ongoing in WP3-4. Therefore, a brief description of the model used to fit the data of section 6 is given in the next paragraphs and the full description is included ad Annex 10.3.

*This project has received funding from the European Union's Horizon 2020 research and innovation programme under the Grant Agreement No **884418***

The evolution of the outlet gas composition in every reacting stage of the CASOH process (i.e. CASOH, Cu oxidation and CuO reduction/$CaCO_3$ calcination) has been represented using a 1-D reactor model. This model simulates a multicomponent system consisting of CO, CO_2, H_2, N_2, O_2, CuO, Cu, $CaCO_3$, CaO and inert materials. Axially dispersed plug flow has been assumed, with negligible inter-particle mass and temperature gradients, a uniform void fraction in the solids bed ($\varepsilon = 0.5$), and an ideal distribution of calcium- and copper-based solids throughout the bed. The model accounts for changes in physical properties due to variations in composition and temperature. Gas-to-solid heat and mass transfer resistances, as well as radial temperature and concentration gradients, are considered negligible due to the high flow rates (up to 120 Nm^3/h) and small particle size ($d_p = 3$ mm). Any possible intraparticle diffusion resistances are accounted for by incorporating average effectiveness factors (η) in the reaction kinetics.

The governing mass and energy balances equations together with the axial mass and heat dispersion coefficients have been included in the mathematical model, which was developed using MATLAB programming and mainly composed of partial differential equations with given initial and boundary conditions and algebraic equations.

First, it is shown the validation of the model for a CASOH stage example conducted in the TRL7 pilot. The kinetics reported by Xu and Froment (10) for the water gas shift reaction was assumed in the model, accompanied by the kinetics for carbonation of CaO assuming the semi-empirical model proposed by Rodriguez et al (11) to interpret pilot plant results using CaO with particle size up to 0.5 mm. As happens with fine particles of limestone, the carbonation of particles of 3 mm is initially limited by the chemical reaction on the entire specific surface of the CaO material. During this period, the solid conversion increases linearly with time until the carbonation is controlled by the diffusion of CO_2 through the solid product layer. Then, the carbonation rate becomes much slower until the maximum carbonation conversion is achieved.

An effectiveness factor (η) of 0.06 included in the model accounts for the internal diffusional resistances during the carbonation of CaO, which corresponds with the empirical value calculated from test carried out previously at smaller scale in TGA and lab-scale packed bed reactors, and already reported in Deliverable 2.3 and by Grasa et al. (2023)(5). Moreover, the volume fraction of CO_2 in the equilibrium during carbonation reaction was estimated using the equation obtained by Baker (20).

In the CASOH stage example outlined in this section, a BFG flow rate of 38 Nm^3/h was introduced, consisting of approximately 21% CO, 22% CO_2, 7% H_2, and 50% N_2. To maintain an S/CO ratio near 2, an additional steam flow of 15 Nm^3/h was supplied Moreover, a nitrogen flow

*This project has received funding from the European Union's Horizon 2020 research and innovation programme under the Grant Agreement No **884418***

of 38 Nm^3/h was fed through the preheaters to ensure safe operation by maintaining a minimum gas flow during high-temperature heating and preventing combustible gas and steam from flowing toward the heaters. The total inlet gas flowrate was then 91 Nm^3/h, resulting in a gas velocity of around 0.5 m/s inside the reactor, with a residence time of approximately 2 seconds (comparable to the expected performance of an industrial-scale CASOH reactor).

As observed in Figure 7.1, during the initial period (pre-breakthrough), the active CaO available in the fixed bed effectively captures nearly all CO_2 fed in the inlet gas and also that produced by the WGS reaction of BFG with steam. Consequently, only a minimal amount of CO_2 and CO (<1 vol%) is detected during this phase, which leads to a CO_2 capture efficiency of around 98%. This CO_2 capture enhances CO conversion and maximizes H_2 production, yielding a product gas composed of approximately 20 vol% H_2 diluted in N_2 (dry basis), as predicted by the equilibrium of the WGS reaction facilitated by the simultaneous CaO carbonation.

As the CO_2 sorbent approaches saturation, H_2 production decreases and the levels of CO and CO_2 in the outlet gas gradually rise (breakthrough period). After 10 minutes of operation (post-breakthrough), CO_2 capture becomes impractical, and the packed-bed reactor functions solely as a WGS reactor, resulting in a gas composition of around 11% vol. H_2, 5% vol. CO and 20% vol. CO_2 in N_2. As can be seen in Figure 7.1, the reactor model closely matches the experimental composition of the product gas during the pre-breakthrough period and it accurately predicts the shape of the breakthrough curve until the solids bed acts as exclusively a WGS reactor

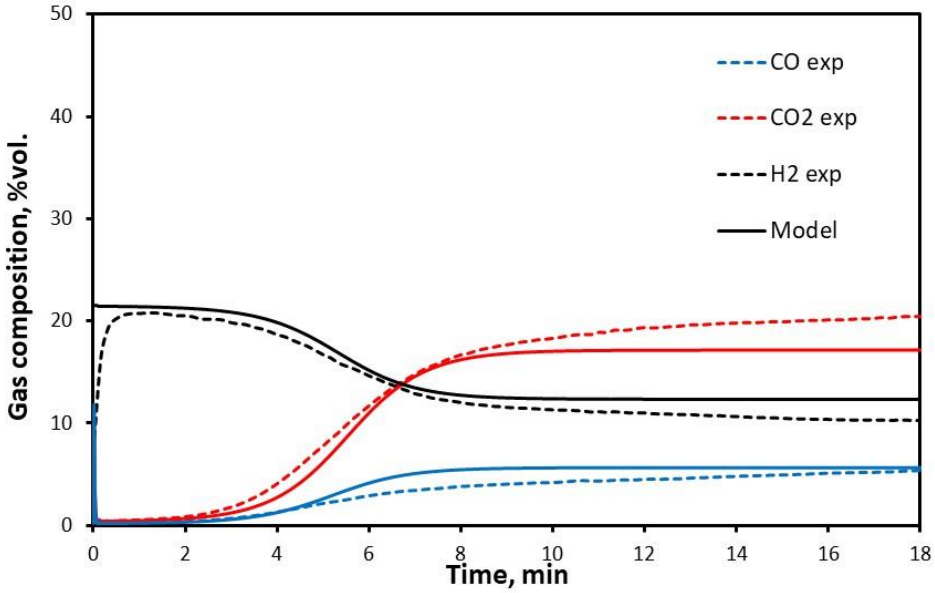

Figure 7.1. Evolution of the product gas composition for an example of CASOH stage including model predictions

*This project has received funding from the European Union's Horizon 2020 research and innovation programme under the Grant Agreement No **884418***

Figure 7.2 shows the strong fit of the model in describing an example of the Cu oxidation stage with air. A Shrinking Core Model (SCM) assuming cylindrical geometry and chemical reaction control without internal diffusion was selected for describing the oxidation of Cu, assuming the kinetic parameters obtained experimentally in TGA and subsequently validated in a lab-scale fixed bed reactor by Grasa et al. (2023)(5). To describe the calcination of $CaCO_3$, it has been used the shrinking core model (SCM) reported by Martinez et al (12), assuming an effectiveness factor (η) of 0.04, which was obtained from the fitting of the calcination curves in TGA reported by Grasa et al (2023)(5). This parameter allows to tackle internal diffusion limitations in the CaO-based solids during calcination.

In this particular oxidation stage example, a flow of 52 Nm^3/h of air mixed with additional 54 Nm^3/h of N_2 was fed into the reactor. This resulted in a total gaseous feed of 106 Nm^3/h with an oxygen concentration of 12% vol. Under these conditions, the maximum gas velocity within the reactor reached 0.6 m/s, leading to a residence time of approximately 1.7 seconds. As can be seen in the figure, during the first 8 minutes of operation, nearly all of the oxygen present in the inlet gas was consumed, with O_2 concentrations dropping to below 0.5% vol. This demonstrates the rapid kinetics of Cu oxidation, even with very short gas residence times. As the oxidation front reached the end of the bed, the O_2 concentration in the outlet gas began rising quickly, reaching the inlet concentration of 12% vol. within just 3 minutes (breakthrough period). This sharp increase confirms the excellent reactivity of the Cu-based material with oxygen. Furthermore, the heat generated during the oxidation reaction caused a partial calcination of the $CaCO_3$ present in the bed. As illustrated in Figure 7.2, CO_2 concentrations in the product gas were initially below 2%, when the temperature of the bed had not yet risen enough to cause significant calcination. However, after 7-8 minutes, CO_2 levels rose sharply, reaching up to 10% vol. in the product gas. Based on the CO_2 measured in the product gas during this phase, it is estimated that nearly 60 moles of the $CaCO_3$ initially present were calcined. Finally, once the O_2 concentration stabilized at 12% vol. in the product gas, matching the inlet concentration, it indicated that all the copper in the bed had been oxidized, marking the completion of the stage.

As happens with the CASOH stage, the model accurately describes the composition of the product gas throughout the entire copper oxidation stage, including the evolution of the breakthrough curve until the end of the stage.

*This project has received funding from the European Union's Horizon 2020 research and innovation programme under the Grant Agreement No **884418***

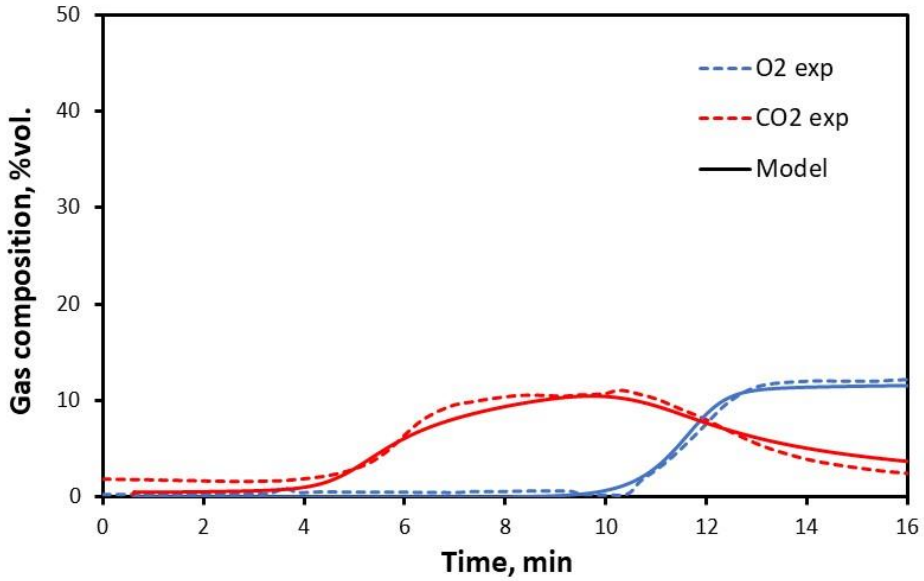

Figure 7.2. Evolution of the product gas composition for an example of Cu oxidation stage including model predictions.

Finally, this section describes the model adjustment for an example of a CuO reduction stage with BFG, in which there was also simultaneous partial calcination of $CaCO_3$. As with the oxidation stage described above, the model considered the CuO reduction kinetics with CO and H_2 obtained by Grasa et al. (2023)(5), which follow an SCM pattern. Likewise, to describe the calcination of $CaCO_3$, it has been used the shrinking core model (SCM) reported by Martinez et al (12), assuming an effectiveness factor (η) of 0.04.

This example stage was preceded by a Cu oxidation period that left the solids bed with a temperature profile ranging between 650 and 750 ºC, which are favourable conditions to initiate a CuO reduction/$CaCO_3$ calcination. In this particular example, a flow of 45 Nm^3/h of BFG diluted with 55 Nm^3/h of N_2 were fed into the reactor, and maintained constant throughout the entire stage. Under these operating conditions, the gas reached a maximum velocity in the reactor of nearly 0.55 m/s, resulting in a residence time within the reactor of approximately 1.8 seconds. As can be seen in Figure 7.3, during the pre-breakthrough period the CO_2 concentration in the product gas reached values between 25 and 30% vol. on a dry basis. Meanwhile, there was an almost complete conversion of H_2 and CO, with both gases registering less than 0.2% vol. on a dry basis in the outlet gas. According to the dilution of the BFG with N_2 in the feed, the CO_2 concentration in the product gas was expected to be around 20% vol. Therefore, the excess of CO_2 observed in the exit gas corresponded to a partial calcination of

*This project has received funding from the European Union's Horizon 2020 research and innovation programme under the Grant Agreement No **884418***

$CaCO_3$. Based on this excess CO_2 observed throughout the pre-breakthrough, it was estimated that approximately 100 moles of $CaCO_3$ were calcined during this period.

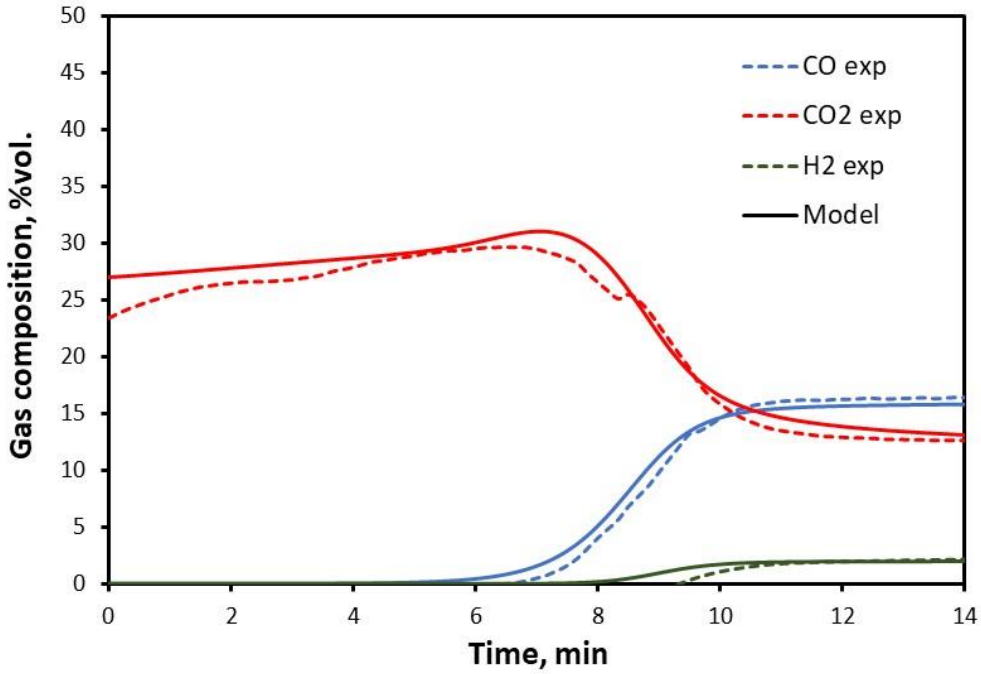

Figure 7.3. Evolution of the product gas composition for an example of CuO reduction with BFG and simultaneous calcination of $CaCO_3$ including model predictions

After 7 minutes of operation, a significant increase in CO and H_2 concentrations (and a decrease in CO_2) was observed in the outlet gas. This fact confirmed that CuO reduction was close to completion. Finally, a rapid breakthrough period of only 3 minutes led to stationary situation in which the composition of the product gas matched that of the inlet gas, marking the stage as complete.

Similarly to the two stages described above, the dynamic curves obtained with the model closely match the trends observed experimentally in the pilot plant. The validation of this model with the preliminary experimental information coming from the pilot represents a first confirmation of the value of said model for scaling up purposes of the CASOH technology, to be confirmed with the future experiments from WP2 towards the end of the project.

*This project has received funding from the European Union's Horizon 2020 research and innovation programme under the Grant Agreement No **884418***

8. Conclusions

The TRL7 CASOH pilot is fully operational, and delivering relevant experimental data to validate and scale up CASOH-based technologies. It can also be a suitable testing platform for other high-temperature solid looping reactions using packed beds with other functional materials.

Unfortunately, many of the risks and challenges faced by developers of CO_2 capture pilots at TRL6-7 materialised for the CASOH pilot. As the experimental work progressed, with increasingly demanding testing conditions (increasing gas flow rates and pressures, increasing temperatures and switching to operations with fuel gases), many issues were revealed that demanded for recommissioning activities and additional repairs. However, these issues were also useful to improve ("learning by doing") the understanding of the pilot dynamics (in particular when operating at high temperatures) as described in Annex 10.1.

All reaction stages involved in the CASOH process have been tested under dynamic conditions, with experimental results consistent with results already available from smaller TRL rigs. The CASOH reaction stage has been shown to achieve deep levels of decarbonisation (up to 98%) of BFG while generating a H_2-rich stream (>40%v when correcting for the N_2 needed in the preheater). The oxidation and reduction stages of the Cu-supported catalyst yield sharp concentration profiles of O_2 and CO_2 that are consistent with the high reactivity of such material under the conditions of the test.

The reactor model available from previous studies of the CASOH reactions at lower TRL is able to fit the new data from the TRL 7 CASOH pilot, with minor tuning to account for the limited information available on the temperatures of the solids. This provides a good basis to expand the experimental works planned in the next and final phase of the C^{4}U project and for future scale up this family of high temperature solid looping technologies.

9. Bibliography / References

1. C^{4}U Project. Advanced Carbon Capture for the Steel Industry integrated in CCUS Clusters. [Internet]. (2020) Available from: https://c4u-project.eu/
2. Fernández, J.R, Abanades, J.C. Overview of the Ca–Cu looping process for hydrogen production and/or power generation. *Curr Opin Chem Eng*. **17**, 1–8 (2017)
3. Alarcón, J.M., Fernández, J.R., CaCO3 calcination by the simultaneous reduction of CuO in a Ca/Cu chemical looping process. Chemical Engineering Science 137, 254–267 (2015).

*This project has received funding from the European Union's Horizon 2020 research and innovation programme under the Grant Agreement No **884418***

4. Zaheer Abbas, S., Fernández, J.R., Amieiro, A., Rastogi, M., Brandt, J., Spallina, V. Lab-scale experimental demonstration of Ca-Cu chemical looping for hydrogen production and in-situ CO_2 capture from a steel mill. *Fuel Processing Technology* **237**, (2022)
5. Grasa, G., Diaz, M., Fernández, J.R., Ameiro, A., Brandt, J., Abanades, J.C. Blast Furnace Gas decarbonisation through Calcium Assisted Steel-mill Off-gas Hydrogen production. Experimental and modelling approach. *Chemical Engineering Research and Design*, **191** (2023) 507–522
6. Diaz, M. Alonso, M., Grasa,G. Fernandez, J.R.The Ca-Cu looping process using natural CO2 sorbents in a packed bed: Operation strategies to accommodate activity decay. *Chemical Engineering Science* 273 (2023)
7. Abanades, J.C., Arias, B., Fernandez, J.R. Vacuum swing calcination process to produce high purity CO_2 from $CaCO_3$. *Patent EP21382495.6* (2021)
8. Abanades, J.C., Arias, B., Fernandez, J.R Steam partial pressure swing calcination process to produce high purity CO_2 from $CaCO_3$. Patent EP22383113 (2022)
9. Fernández, J.R., Abanades, J.C., Diaz, M., Mendez, A., Alonso, M., Grasa, G., et al. The design of the CASOH process pilot to test the decarbonisation of blast furnace gas using the Ca-Cu chemical loop. The *Greenhouse Gas ControlTechnology Conference, GHGT16 Communication,* (2022)
10. Xu, J., Froment, G.F. Methane steam reforming, methanation and water-gas shift: I. Intrinsic kinetics. *AIChE journal* **35**, 88-96 (1989).
11. Rodríguez, N., Alonso, M., Abanades, J.C. Experimental investigation of a circulating fluidized-bed reactor to capture CO_2 with CaO. *AIChE journal* **57**, 1356-1366 (2011).
12. Martínez, I., Grasa, G., Murillo, R., Arias, B., Abanades, J.C. Kinetics of calcination of partially carbonated particles in a Ca-looping system for CO_2 capture. *Energy Fuels* **26** (2), 1432-1440 (2012).
13. Díez-Martín, L., et.al. Determination of the oxidation kinetics of high loaded CuO-based materials under suitable conditions for the Ca/Cu H_2 production process. *Fuel* **219**, 76-87 (2018).
14. Díez-Martín, L., Martínez, I., Grasa, G., Murillo, R. Investigation of the reduction kinetics of high loaded CuO-based materials suitable for the Ca/Cu looping process. *Fuel* **230**, 376-389 (2018).
15. Ergun, S. Fluid flow through packed columns. *Chem. Eng. Prog.* **48**,89-94 (1952).
16. Edwards, M.F., Richardson, J.F., 1968. Gas dispersion in packed beds. *Chemical Engineering Science* **23**, 109-123 (1968).
17. Vortmeyer, D., Berninger, R., Comments on the paper, theoretical prediction of effective heat transfer parameters in packed beds by Anthony Dixon and D. L. Cresswell [AIChE J., 25, 663 (1979)]. *AIChE Journal* **28**, 508-510 (1982).

*This project has received funding from the European Union's Horizon 2020 research and innovation programme under the Grant Agreement No **884418***

18. Gunn, D.J., Axial and radial dispersion in fixed beds. *Chemical Engineering Science* **42**, 363-373 (1987).
19. Twigg, M.V., 1989. Catalyst Handbook , Doing Narrative Research. Wolfe Publishing Ltd, United Kingdom.
20. Baker, E. The calcium oxide-carbon dioxide system in the pressure range 1-300 atm. *J. Chem. Soc.* (Resumed), 464-470. (1962).
21. Fernández, J.R., Spallina, V., Abanades, J.C. Advanced Packed-Bed Ca-Cu Looping Process for the CO_2 Capture from Steel-Mill Off Gases. *Frontiers in Energy Research* **8**(146), (2020).

*This project has received funding from the European Union's Horizon 2020 research and innovation programme under the Grant Agreement No **884418***

10. ANNEXES

10.1 Pilot testing after site acceptance test (from Nov 2023)

As indicated in the Introduction and Scope section, the purpose of this first Annex is to report, in a chronological order, the works carried out during the early test on the integrated CASOH pilot. The beginning of testing campaigns started after the site or factory acceptance test led by AM R&D (D2.4, submitted on the 1st of Nov 2023).

In early November 2023, during the first test blowing N2 through the entire pilot, it was found that there was a leakage in some of the flanges of the reactor. Three re-tighten campaigns by an external certified contractor (see also Figure 5.4), with increasing levels of torque on the bolts (up to the final 4000 N/m, that required the change of the bolts) were needed. They were carried out between November 2023 and January 2024. During the leakage test carried out after each re-tightening, it was noticed that 10 positioners of the gas valves were not properly installed, and the valves where not providing a full sealing when in off position. Furthermore, they did not return their real position to the control system. This required a change in some of the valves and a readjustment of all positioners, works carried out by GasLab technical support staff at AM R&D.

During first test in January 2024, after the gas leakages in reactor had been solved, the air compressor failed, due to an error in its controller, and it was necessary to disassemble the control module and send it to the manufacturer. The operation of the pilot relayed on the use of N_2 as non-fuel gas operations (available at the CASOH pilot site as an industrial process gas from the AM factory, at a maximum rate up to 130 Nm^3/h). The mass flow controller and % of opening of the controlling valve of the N_2 were calibrated as shown in Figure 10.1.1, using a Pitot tube.

*This project has received funding from the European Union's Horizon 2020 research and innovation programme under the Grant Agreement No **884418***

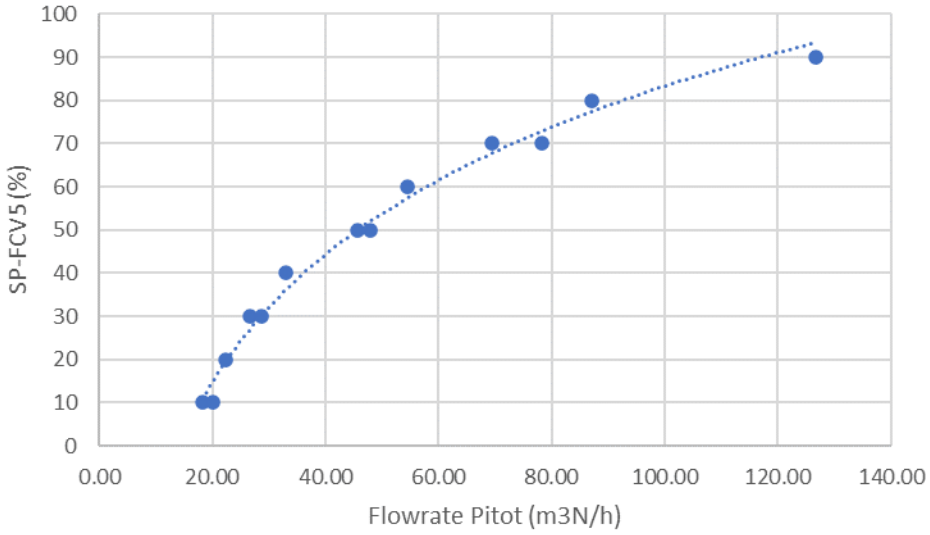

Figure 10.1.1. Calibration curve of the percentage opening of the valve vs Nitrogen flowrate measured by a Pitot.

During new preheating test of the pilot, it was detected that the water refrigeration circuit (used in a closed loop to feed the heat exchanger that cools the hot gases coming from the CASOH reactor), experienced stability problems, with random changes in water flow rates. To solve this issue, changes in the refrigeration circuit were introduced by changing the faulty pump, adding several valves (that help during the charging/de-charging of water in the circuit) and installing an expansion vessel for absorbing the dilatations during the operation. A new PI&D for this system was generated (see Figure 10.1.2) and the new circuit was re-commissioned in March 2024.

*This project has received funding from the European Union's Horizon 2020 research and innovation programme under the Grant Agreement No **884418***

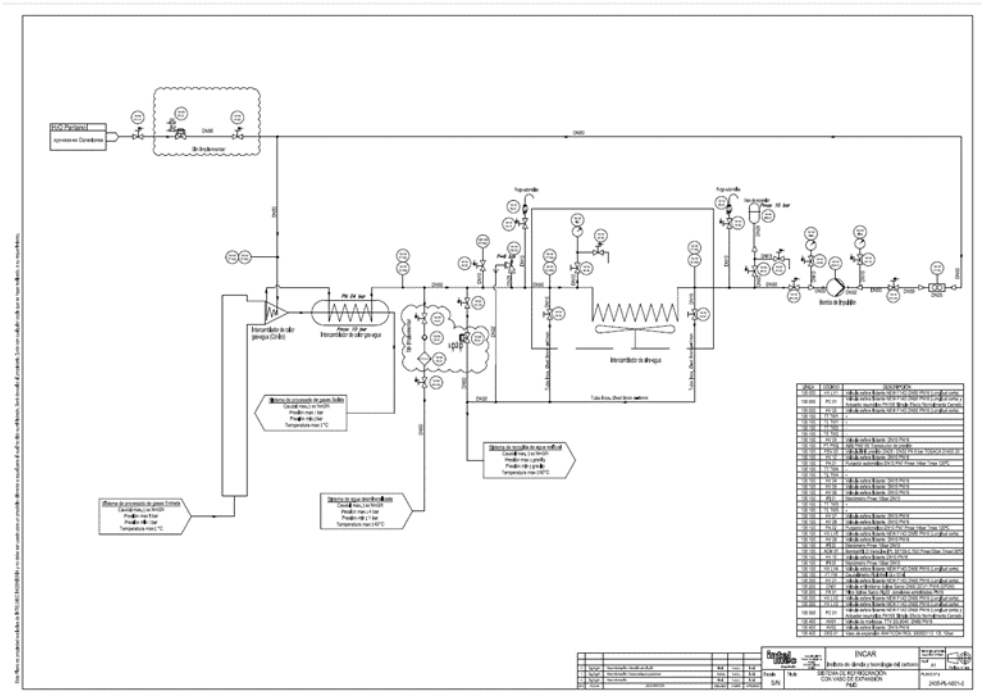

Figure 10.1.2. New P&D for refrigeration system

On the other hand, also at the beginning of February, and during preheating test to evaluate heat losses and test high temperature conditions, a major problem with the Kanthal electric pre-heater was found. The pre-heater was disassembled and the Technical Service of CSIC checked it, suggesting that the failure/breakage was clearly located in a single point of the heater (see Figure 10.1.3) while the rest had no indication of having reached the high temperatures characteristic of the heating elements in this type of preheaters. To avoid further delays in the experimental works, the preheater was eventually repaired by Technical Service of CSIC.

*This project has received funding from the European Union's Horizon 2020 research and innovation programme under the Grant Agreement No **884418***

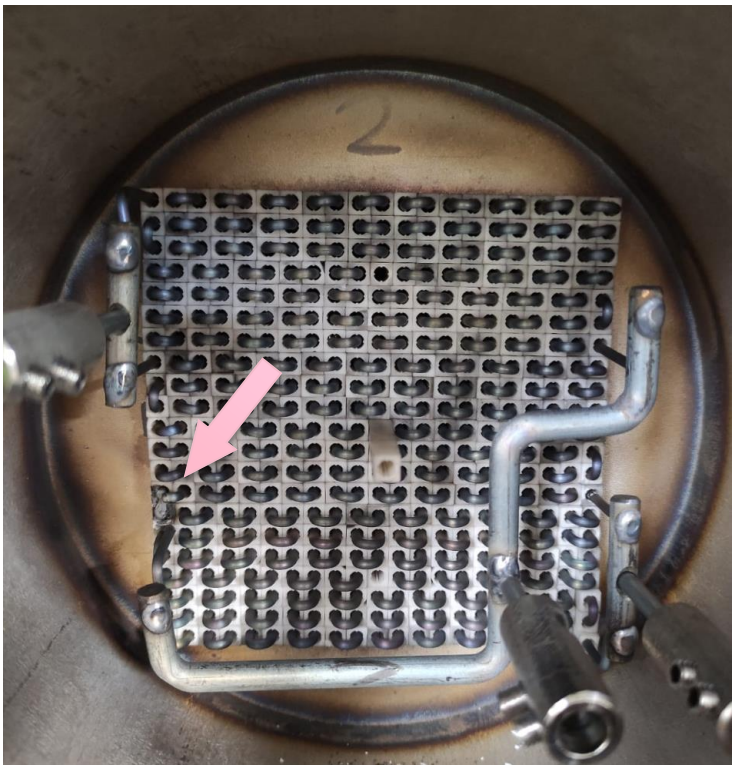

Figure 10.1.3. Internal view of the preheater indicating the point of failure.

In parallel with the works to address and repair the preheater, several pressure test were carried out during February to identify small leakages. In order to find them, the plant was sectorize by installing blind joints in certain points. Figure 10.1.4 shows two screenshots for pressure test in N_2 and CO_2 lines up to preheaters after all leakages were fitted in these sectors. During the leakage test in the second part of the plant (between preheaters and the gas exits) it was found that a joint in the spool between pre-heaters and reactor had not been adequately chosen and installed. It was necessary to replace it, including new bolts and screws as needed in such high temperature part of the pilot.

*This project has received funding from the European Union's Horizon 2020 research and innovation programme under the Grant Agreement No **884418***

(a)

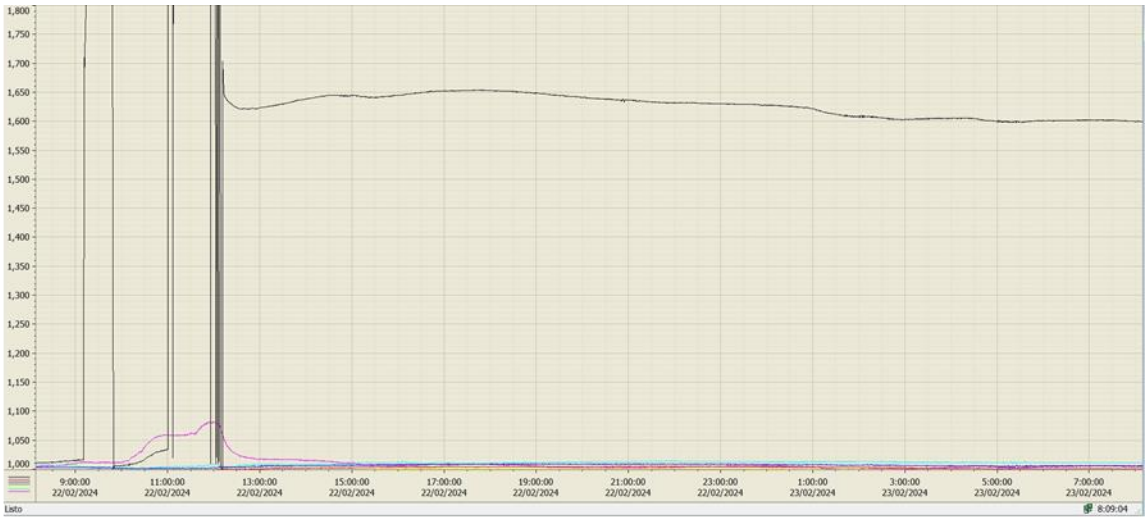

(b)

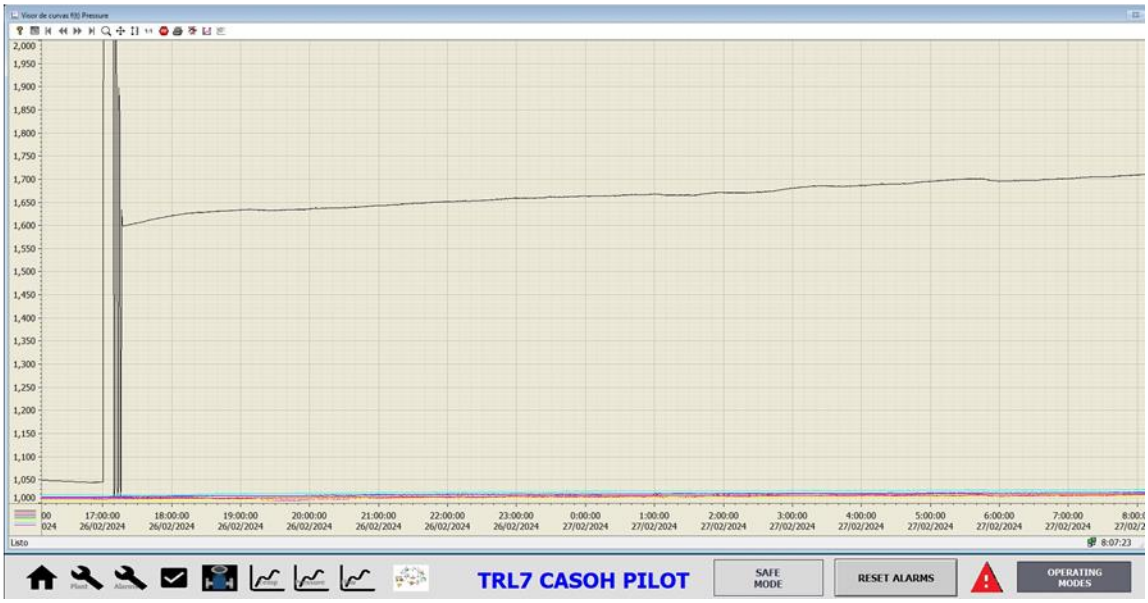

Figure 10.1.4. Pressure test carried out in the lines (a) of N_2 and (b) of CO_2 up to the inlet of pre-heaters once the plant was sectorized.

Also, at the end of February, the controller of the air compressor had been repaired by the manufacturer and was re-installed in the pilot plant. At that point, the compressor was fully functional at the beginning of March when operating it in manual mode, but Issues were still

*This project has received funding from the European Union's Horizon 2020 research and innovation programme under the Grant Agreement No **884418***

present with the communication module of the compressor and the control system of the pilot, and it was not possible to operate it from the control system.

A calibration of the air mass flowmeter and the opening of the valve control was carried out by using the Pitot in March. Figure 10.1.5 shows the curve of the air flowrate measured by Pitot as a function of the open percentage of the control valve.

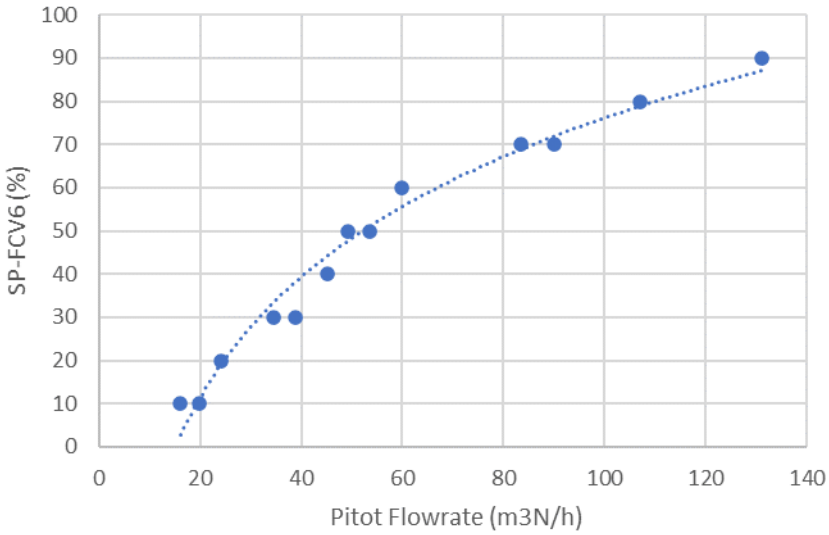

Figure 10.1.5. Calibration curve of the percentage opening of the valve vs Air flowrate measured by a Pitot.

In order to calibrate the CO_2 flowmeter, it was used the analysers for estimating the CO_2 flowrate when mixtures of N_2 and CO_2 were measured. The figure 10.1.6 shows the estimated CO_2 flowrate by the analyzers as a function of the % opening control valve.

*This project has received funding from the European Union's Horizon 2020 research and innovation programme under the Grant Agreement No **884418***

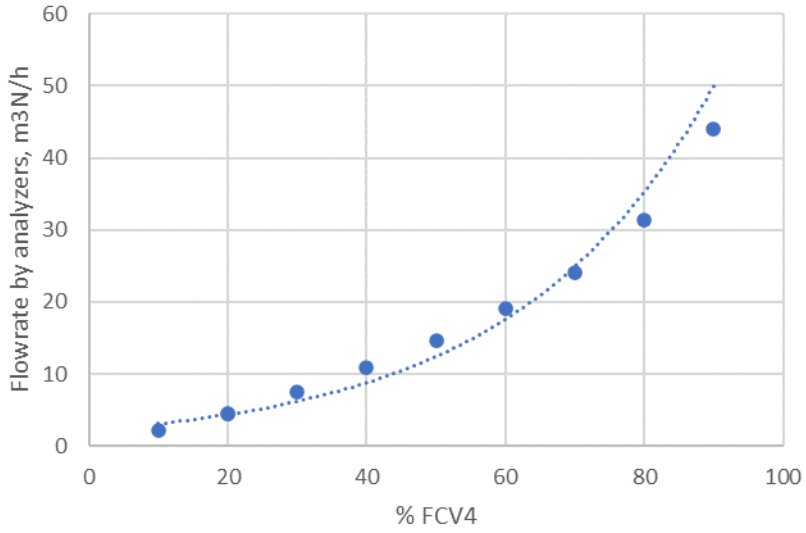

Figure 10.1.6. Calibration curve of the percentage opening of the valve vs CO_2 flowrate estimated through analysers measurements.

Due to changes in the thermocouple types, a calibration of the control thermocouples of the pre-heaters (TH1, TH2 and TH3) as well as of the thermocouples of the multipoint probes of the reactor (TR1, TR2 and TR4-6) was carried out in March. Figure 10.1.7 shows the experimental measurements of thermocouples versus the reference temperature generated by a pattern generator in the entire range of measurement.

*This project has received funding from the European Union's Horizon 2020 research and innovation programme under the Grant Agreement No **884418***

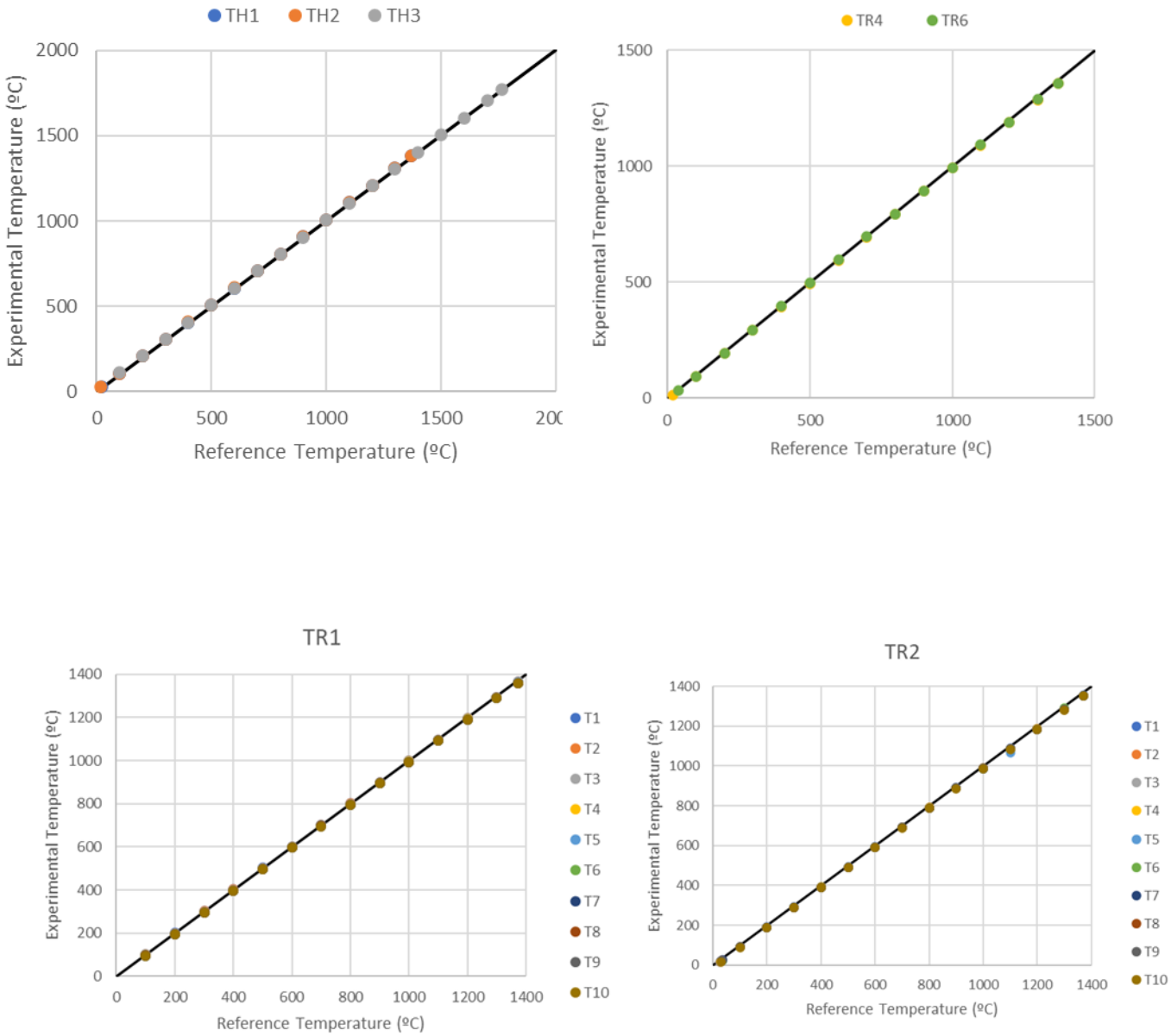

Figure 10.1.7. Calibration of thermocouples of the preheaters and reactor. Upper left: control thermocouples of the preheaters. Upper right: TR4-6 reactor multipoint thermocouple. Lower: reactor multipoint thermocouples in TR1 and TR2.

*This project has received funding from the European Union's Horizon 2020 research and innovation programme under the Grant Agreement No **884418***

At the end of April, the repaired pre-heater was reinstalled, and a test of heating was carried out at the beginning of May. Figure 10.1.8 shows the comparison between the experimental power of each preheater (lines) and the power of each preheater estimated through the heat balance (dash lines).

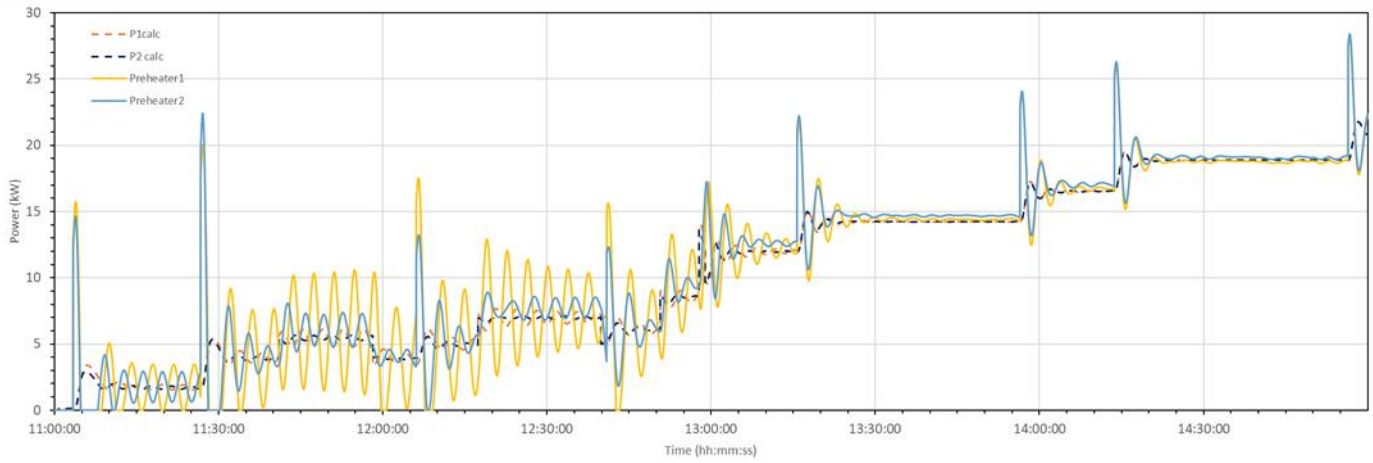

Figure 10.1.8. Power of preheaters during a heating test. Experimental (lines), estimated through a heat balance (dash lines).

From April to the beginning of May, the control system of the torch was re-integrated in the control of the plant. As it was detected that the mass flowmeter of BFG did not work properly, a calibration of the control valve was carried out by using the gas flowmeter to the torch. Figure 10.1.9 shows the calibration of the % opening the control valve.

*This project has received funding from the European Union's Horizon 2020 research and innovation programme under the Grant Agreement No **884418***

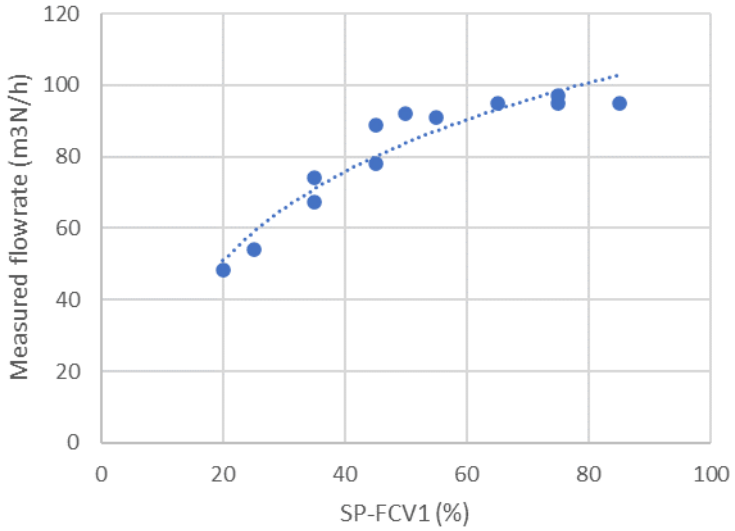

Figure 10.1.9. Measured flowrate of BFG by gas flowmeter of the torch as a function of the % opening of control valve.

The first time that BFG was fed to the reactor bed of solids was on 13/05/2024. A reduction, CASOH without steam and oxidation stages were carried out. Figure 10.1.10 shows an overview of all signals that were recorded during such first test involving fuel gas decarbonisation.

*This project has received funding from the European Union's Horizon 2020 research and innovation programme under the Grant Agreement No **884418***

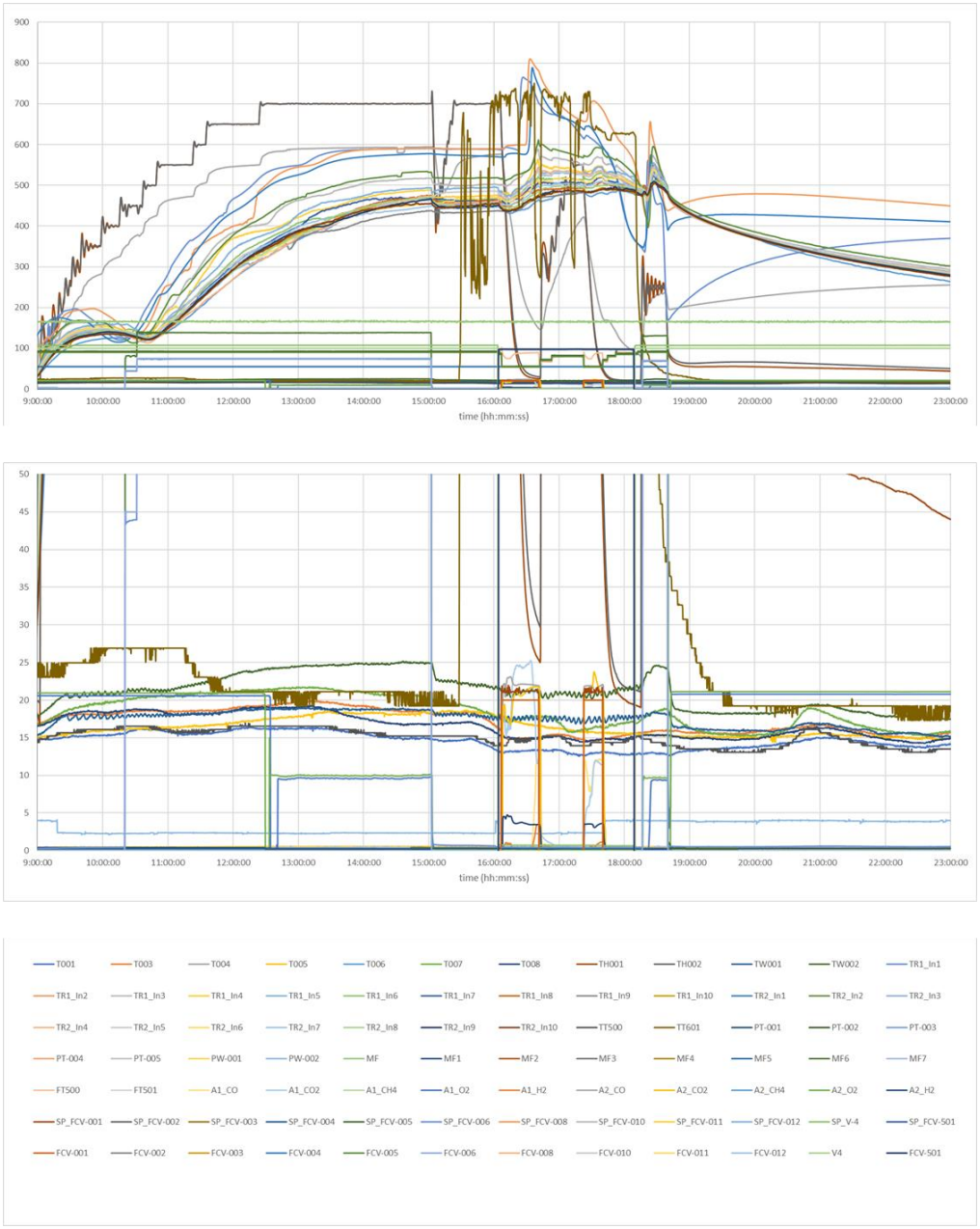

Figure 10.1.10. Overview of the signals recorded during the first test decarbonising BFG with a partially precalcined bed containing CaO (<10% Ca conversion). The graph in the middle shows a zoom of some signals in the datalog.

The control system recorded at this point 87 signals from the pilot plant (temperatures, pressures, gas compositions, flowmeters, valve status, power input to preheater etc). The upper

*This project has received funding from the European Union's Horizon 2020 research and innovation programme under the Grant Agreement No **884418***

graph shows the signals at the total range whereas the bottom graph shows a zoom of the variables during all the test.

During this test, the heating up stage lasted 6 h. Figure 10.1.11. shows the variation of temperatures in the solid bed, the used gas flowrates, the variation of pressures and the experimental used power for each pre-heater compared with the estimated power though the heat balance in the pre-heaters.

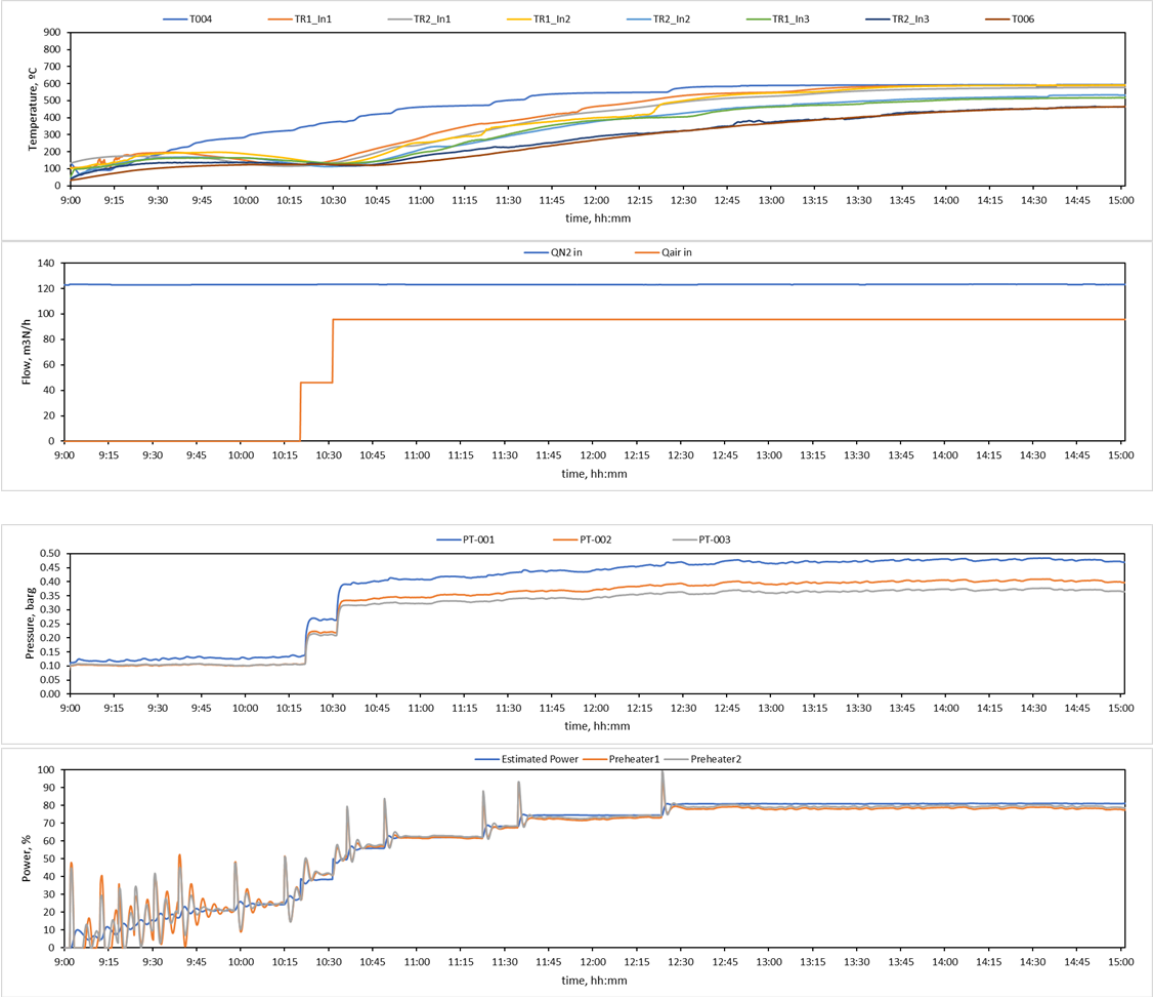

Figure 10.1.11. Variation of temperatures, used gas flowrates, variation of pressures and used power of each pre-heaters as well as estimated power through heat balance during the heating up stage of the pilot plant.

*This project has received funding from the European Union's Horizon 2020 research and innovation programme under the Grant Agreement No **884418***

At the beginning of the experiment, the heating was carried out by using a gas flow rate of 123 m3N/h of Nitrogen (maximum flow from the N_2 process supply line). In order to increase the heating rate of the reactor, the gas flowrate was increased to 220 m^3N/h by adding air at around 10:30 h from the compressor. Accordingly the pressure at the inlet of the reactor increased from an average value of 0.13 barg at the beginning to 0.39 barg at 10:30. Then, the pressure at the inlet of the reactor was increased slowly from this point to a value around 0.484 barg at the end of the heating stage, whereas the bed temperatures increased from an average value of 125 ºC at 10:30 to a range of values between 591 ºC and 517 ºC. The power supplied by the preheaters was increased from 40 % at 10:30 to 80 %.

After a purge period, a reduction stage was carried out by using BFG. Figure 10.1.12. shows the evolution of the relevant variables during this stage.

A mixture of 52 m^3N/h of N_2 with 36 m^3N/h of BFG was fed to the reactor (Figure 10.1.12.(c)) during all the stage. The average measured BFG gas concentrations were 22 %vol. of CO, 21.7 %vol. of CO_2 and 3.5 %vol. of H_2 (Figure 10.1.12 (e)). The pre-heaters were switched off at the initial of the stage. After 8 min of the injection, the first thermocouple in the bed of reactor (around 0.5 m from the inlet) started to increase in temperature up to a maximum of 760 ºC after 10 min of injection (Figure 10.1.12. (a)). Then, the rest of the bed increased in temperature once the front of reaction achieved the point of the thermocouples. The maximum temperature achieved was 806 ºC after 17 min of reaction. The average CO_2 gas concentration increased to a maximum value of 25.25 %vol. after 17 min of reaction (Figure 10.1.12.(d)) due to the calcination and the reduction of copper. Also, measured CO and H_2 gas concentrations were 0%vol. due to the reduction reaction conditions. After 20 min of reaction, CO and H_2 gas concentration at the exit of reactor increased to the values of the inlet, whereas CO_2 concentration decreased to the value of the inlet concentration being the calcination and the reduction reactions stopped.

*This project has received funding from the European Union's Horizon 2020 research and innovation programme under the Grant Agreement No **884418***

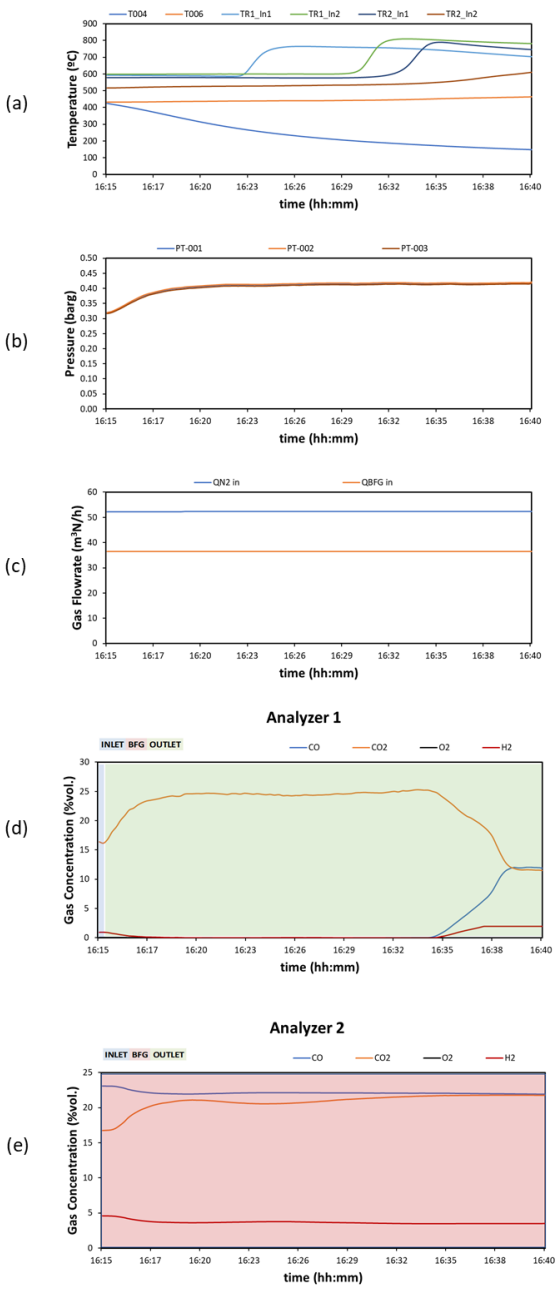

Figure 10.1.12. Reduction stage. (a). Evolution of bed temperatures, (b) evolution of pressures at the inlet of reactor, (c) used gas flowrates (d) gas compositions measured by analyzer 1 and (e) gas composition measured by analyzer 2.

*This project has received funding from the European Union's Horizon 2020 research and innovation programme under the Grant Agreement No **884418***

After the reduction stage, a nitrogen gas flowrate was fed to the reactor and the preheaters were switched on in order to heat up the bottom of the bed. Then a partial CASOH, without steam addition but attempting decarbonisation by capturing CO_2 with CaO, was carried out. However, due to the lack of steam and the small amount of free CaO in the bed the carbonation reaction was negligible in this first attempt. After this stage, and a purge with nitrogen, an oxidation stage was carried out in an attempt to calcine a higher fraction of the material. Figure 10.1.13. shows the relevant variables during this stage.

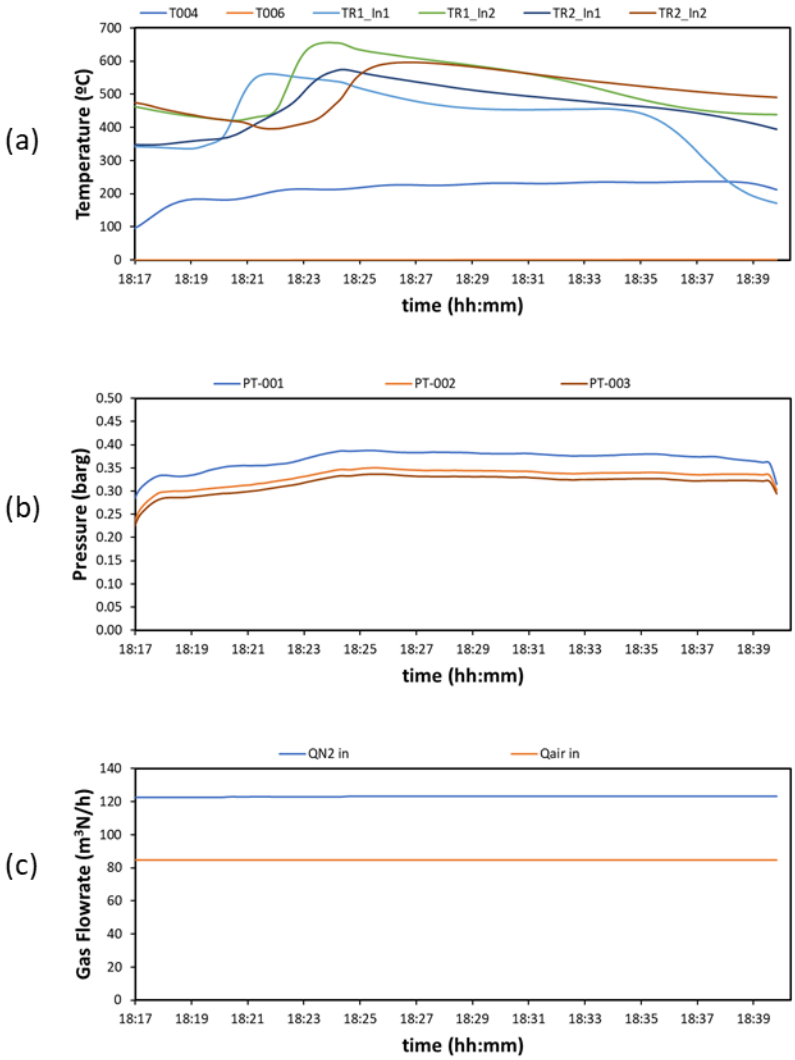

Figure 10.1.13. Oxidation stage. (a) Evolution of temperatures in the bed (b) evolution of pressures at the inlet of the reactor (c) used gas flowrates.

*This project has received funding from the European Union's Horizon 2020 research and innovation programme under the Grant Agreement No **884418***

A mixture of 125 Nm^3/h of nitrogen and 85 Nm^3/h of air was fed to the reactor (Figure 10.1.13. (c)). After 5 min of injection the first thermocouple in the bed of reactor (TR1_LN1) detected an increase in temperature from 347 °C to 560 °C (Figure 10.1.13 (a)). The maximum temperature achieved during this stage was 656 °C at 0.65 m from the bottom of the bed after 8 min of injection. The oxidation reaction seemed to be finished after around 18 min, noticeable from the drop in temperatures in the bed and the product gas compositions.

The rest of the test involving complete CASOH reactions and oxidation and reduction stages are described in section 6 and 7. Finally, Table 10.1.1 summarizes the activity days between the factory acceptance test (1st November 2023) and September 2024. Green days are testing days, total hours of test on the pilot, involving acquisition of relevant data for operation; orange days are days involving testing works on the pilot, as necessary to reach relevant conditions for operation whereas white days are idle days with no operations on the pilot.

*This project has received funding from the European Union's Horizon 2020 research and innovation programme under the Grant Agreement No **884418***

Table 10.1.1. AM R&D-CSIC operating days between site or Factory acceptance test and the end of August 2024. Green days: testing on pilot, Orange days: re-commisioning and pre-test and white days: idle

Month/Year	1	2	3	4	5	6	7	8	9	10	11	12	13	14	15	16	17	18	19	20	21	22	23	24	25	26	27	28	29	30	31
Nov/23																															
Dec/23																															
Jan/24																															
Feb/24																															
March/24																															
April/24																															
May/24																															
Jun/24																															
Jul/24																															
Aug/24																															

*This project has received funding from the European Union's Horizon 2020 research and innovation programme under the Grant Agreement No **884418***

10.2 Description of the reactor model as tuned to the TRL7 experimental results

The packed-bed reactor operation at TRL7 has been simulated by means of a pseudo-homogeneous reactor model adopting the following assumptions: plug flow pattern with axial mass and thermal dispersion and negligible radial gradients, ideal gas behaviour, adiabatic conditions, absence of temperature and concentration gradients at inter-particle level, uniform particle size and void fraction, and perfect mixing of the Ca- and Cu-based solids in the bed. Mass and energy balances include the kinetics reported by Xu and Froment (10) for the water gas shift reaction, together with the kinetics for carbonation/calcination and oxidation/reduction reactions described in Tables 2-3. The volume fraction of CO_2 in the equilibrium during calcination and carbonation reactions has been estimated using the equation obtained by Baker (20).

According to the experimental results obtained in TGA and reported in Deliverable 2.3 and in two recent publications (5,6), the carbonation of CaO-based particles can be accurately described using a homogeneous reaction model (5,6) that includes an effectiveness factor of 0.06 to account for the internal diffusional resistances. The calcination reaction can be well represented by means of a Shrinking Core Model (SCM) (12), including an effectiveness factor of 0.04 to tackle internal diffusion limitations in the solid during calcination (5,6). With respect to the redox reactions in the Cu-based material, a Shrinking Core Model (SCM) assuming cylindrical geometry and chemical reaction control without internal diffusion (13,14) is able to describe accurately both reduction and oxidation experimental curves. The reactor model aforementioned has been validated with experimental data from all the reaction stages and bed compositions of the CASOH process, also investigated at TRL4 and TRL3 as described in (5, 4).

The mathematical model has been solved using MATLAB programming by converting the multi-component system into a set of ordinary differential equations (ODE) using backward finite differences with initial and boundary conditions. The resulting stiff ODE system has been solved using the *"ode15s" function*. The set of partial differential equations and algebraic equations included in the model are listed in Table 1. The kinetic equations and parameters to describe reaction rates and equilibrium conditions are included in Table 2 and Table 3.

*This project has received funding from the European Union's Horizon 2020 research and innovation programme under the Grant Agreement No **884418***

Table 1. Mass and Energy Balances Used in the pseudo-homogeneous reactor model

Component mass balance

$$\varepsilon\frac{\partial C_i}{\partial t} = -u_g\frac{\partial}{\partial z}\left(D_{eff}\frac{\partial C_i}{\partial z}\right) + \eta(1-\varepsilon)r_i$$

Energy balance

$$\left((1-\varepsilon)\rho_s C_{ps} + \varepsilon\rho_g C_{pg}\right)\frac{\partial T}{\partial t} = -u_g\rho_g C_{pg}\frac{\partial T}{\partial z} + \frac{\partial}{\partial z}\left(\lambda_{eff}\frac{\partial T}{\partial Z}\right) - \sum\eta_i(1-\varepsilon)H_{ri}r_i - U(4/d_r)(T-T_w)$$

Momentum balance (15)

$$\frac{dP}{dz} = -150\frac{u_g(1-\varepsilon)^2}{{d_P}^2\varepsilon^3} + 1.75\frac{\rho_g {u_g}^2(1-\varepsilon)}{d_P\varepsilon^3}$$

Axial mass and heat dispersion coefficients (16-18)

$$D_{eff} = \left(\frac{0.73}{R_e S_C} + \frac{0.5}{\varepsilon + \frac{9.7\varepsilon^2}{R_e S_c}}\right)u_g d_P \; ; \quad \lambda_{eff} = \lambda_{0bed} + \frac{R_e P_r k_g}{Pe_{az}} + \frac{{R_e}^2 {P_r}^2 {k_g}^2}{6(1-\varepsilon)N_u} \; ; \quad N_u = 2 + 1.8{R_e}^{0.5}{P_r}^{0.33}$$

$$\lambda_{0bed} = \left(\frac{k_s}{k_g}\right)^{0.28-0.757\log(\varepsilon)-0.057\log(k_s/k_g)} \; ; \; Pe_{az} = \frac{2p}{1-p}; \quad p = 0.17 + 0.29e^{(-24/R_e)}$$

*This project has received funding from the European Union's Horizon 2020 research and innovation programme under the Grant Agreement No **884418***

Table 2. Kinetic equations and parameters included in the reactor model (10,19).

$$R_1 = \frac{1}{(DEN)^2}\frac{k_1}{P_{H_2}}\left(P_{CO}P_{H_2O} - \frac{P_{CO_2}{P_{H_2}}^3}{K_3}\right)$$

$$DEN = 1 + K_{CO}P_{CO} + K_{H_2}P_{H_2} + K_{H_2O}\frac{P_{H_2O}}{P_{H_2}}$$

$$r_{H_2O} = -R_1$$

$$r_{H_2} = +R_1; \quad r_{CO_2} = +R_1$$

$$r_{CO} = -R_1$$

$$K_1 = exp(-0.29353Z^3 + 0.63508Z^2 + 4.1778Z + 0.31688)$$

$$Z = \frac{1000}{T} - 1$$

$$k_1 = 7.558exp\left(\frac{63130}{R}\left(\frac{1}{T} - \frac{1}{648}\right)\right) \quad \frac{kmol}{kg_{catalyst}\ bar\ h}$$

$$K_{H_2O} = 0.4152exp\left(\frac{88680}{R}\left(\frac{1}{T} - \frac{1}{823}\right)\right)$$

$$K_{CO} = 40.91exp\left(\frac{70650}{R}\left(\frac{1}{T} - \frac{1}{648}\right)\right) \quad bar^{-1}$$

$$K_{H_2} = 0.0296exp\left(\frac{82900}{R}\left(\frac{1}{T} - \frac{1}{648}\right)\right) \quad bar^{-1}$$

*This project has received funding from the European Union's Horizon 2020 research and innovation programme under the Grant Agreement No **884418***

Table 3. Kinetic equations and parameters included in the reactor model

Carbonation (5,11,20)

$$\frac{dX_{carb}}{dt} = \eta_{carb} k_{carb} (X_{max} - X) \cdot (v_{CO2} - v_{CO2,eq});\ \eta_{carb} = 0.06;\quad k_{carb} = 0.35\ s^{-1};\ r_{carb} = \frac{\eta}{M_{CaO}} \left(\frac{dX}{dt}\right)$$

$$v_{CO2,eq} = 4.137 \cdot 10^{7} exp\left(\frac{-20474}{T}\right)$$

Calcination (5,12,20)

$$\frac{dX_{cal}}{dt} = \eta_{cal}\, k_{cal} (1 - X_{cal})^{\frac{2}{3}} \left(C_{CO_{2,eq}} - C_{CO_2}\right);\ \eta_{cal} = 0.04\ ;\ r_{cal} = \frac{\rho_{CaCO_3} 1000}{M_{CaCO_3}} \frac{dX_{cal}}{dt}$$

$$k_{cal} = k_0 \cdot e^{\frac{-Ea}{R \cdot T}};\ k_0 = 2.52 \cdot 10^2\ \mathrm{m^3/(mol\ s)};\quad E_{act} = 91.7 \cdot 10^2\ J\ mol^{-1};$$

$$C_{CO_{2,eq}} = \frac{5.045 \cdot 10^{11}}{T} exp\left(\frac{-20474}{T}\right)$$

Oxidation or Reduction (13,14)

$$\frac{t}{\tau_i} = 1 - (1 - X_{oxi\ or\ red})^{\frac{1}{2}}\ ;\quad \tau_i = \frac{\rho_b L_p}{b_i k_{si} C_{gi}^n}\ (i = CO, CH_4\ or\ O_2)\ ;\ kr_i = kr_{0i} \cdot e^{\left(\frac{-E_{act,red,oxi}}{RT}\right)}$$

Nomenclature:

b	$stoichiometric\ coefficient\ in\ particle\ reaction\ model$
C_{CO_2}	$concentration\ of\ CO_2\ in\ the\ gas\ phase, kmol\ m^{-3}$
$C_{CO_{2,eq}}$	$equilibrium\ concentration\ of\ CO_2\ , kmol\ m^{-3}$
C_i	$concentration\ of\ the\ component\ i\ in\ the\ reactor, kmol\ m^{-3}$
$C_{i,in}$	$concentration\ of\ the\ component\ i\ in\ the\ feed, kmol\ m^{-3}$
$C_{i,0}$	$initial\ concentration\ of\ the\ component\ i, kmol\ m^{-3}$
C_{gi}	$concentration\ for\ gas\ i\ in\ particle\ model, mol\ m^{-3}$
$C_{p,g}$	$specific\ heat\ capacity\ of\ the\ gas, kJ\ kg^{-1}\ K^{-1}$
$C_{p,s}$	$specific\ heat\ capacity\ of\ the\ solid, kJ\ kg^{-1}\ K^{-1}$
D_{eff}	$axial\ mass\ dispersion\ coefficient, m^2 s^{-1}$
d_p	$particle\ diameter, m$

*This project has received funding from the European Union's Horizon 2020 research and innovation programme under the Grant Agreement No **884418***

d_r	$inner\ diameter\ of\ the\ reactor, m$
$E_{act,cal}$	$activation\ energy\ calcination\ reaction, J\ mol^{-1}$
$E_{act,red,ox}$	$activation\ energy\ reduction, or\ oxidation\ reaction, kJ\ mol^{-1}$
H_{ri}	$enthalpy\ reaction\ of\ gas\ component\ i, kJ\ mol^{-1}$
$k_{0,cal}$	$preexponential\ factor\ of\ the\ CaCO_3\ calcination\ reaction, m^3\ mol^{-1} s^{-1}$
k_{cal}	$reaction\ rate\ constant\ of\ the\ CaCO_3\ calcination, kJ\ mol^{-1}$
k_{carb}	$reaction\ rate\ constant\ of\ the\ CaO\ carbonation, s^{-1}$
k_g	$thermal\ conductivity\ of\ the\ gas, kW\ m^{-2}\ K^{-1}$
k_1	$rate\ constant\ of\ reaction\ 1, (kmol/kg\ bar\ h)$
k_{ri}	$kinetic\ constant\ for\ the\ reaction\ with\ gas\ i\ (i = CO, CH_4, O_2), mol^{(1-n)} m^{(3n-2)} s^{-1}$
k_{r0i}	$pre-exponential\ factor\ in\ kinetic\ constant\ for\ the\ reaction\ with\ gas\ i\ (i = CO, CH_4, O_2), mol^{(1-n)} m^{(3n-2)} s^{-1}$
k_s	$thermal\ conductivity\ of\ the\ solids, kW\ m^{-2}\ K^{-1}$
K_i	$adsorption\ constant\ of\ component\ i, i = CO, H_2\ \ bar^{-1}; i = H_2O\ dimensionless$
K_1	$equilibrium\ constant\ of\ reaction\ 1\ dimensionless$
L	$reactor\ length, m$
L_p	$Cu\ pellet\ radius, m$
M_{CaCO_3}	$molar\ mass\ of\ CaCO_3, kg\ kmol^{-1}$
n	$reaction\ order$
N_u	$Nusselt\ number, dimensionless$
P	$pressure, bar$
Pe_{az}	$Peclet\ number, dimensionless$
P_{in}	$pressure\ at\ the\ reactor\ entrance, bar$
P_r	$Prandt\ number, dimensionless$
R_j	$Rate\ of\ reaction\ j\ (j=1)\ kmol/kg\ s$
R	$ideal\ gas\ constant, kJ\ kmol^{-1}\ K^{-1}$
R_e	$Reynolds\ number, dimensionless$
r_{cal}	$reaction\ rate\ of\ CaCO_3\ calcination, mol\ m^{-3} s^{-1}$
r_{carb}	$reaction\ rate\ of\ CaO\ carbonation, kmol\ kg_{cat}^{-1} s^{-1}$
r_i	$reaction\ rate\ of\ component\ i, kmol\ kg^{-1} s^{-1}$
S_c	$Schmidt\ number, dimensionless$
T	$temperature, K$
T_{s_0}	$initial\ temperature\ of\ the\ solids\ in\ the\ reactor, K$
$T_{g_{in}}$	$feed\ gas\ temperature, K$
T_w	$reactor\ wall\ temperature, K$
X_{cal}	$fractional\ calcination\ conversion\ of\ CaCO_3, dimensionless$

*This project has received funding from the European Union's Horizon 2020 research and innovation programme under the Grant Agreement No **884418***

X_{carb}	$fractional\ carbonation\ conversion\ of\ CaO, dimensionless$
X_{ox}	$fractional\ oxidation\ conversion\ of\ Cu, dimenionless$
X_{red}	$fractional\ reduction\ conversion\ of\ CuO, dimenionless$
X_{max}	$maximum\ fractional\ carbonation\ conversion\ of\ CaO, dimensionless$
z	$axial\ coordenate\ in\ bed, m$

Greek Letters

ε	$bed\ void\ fraction, dimensionless$
ρ_{CaCO_3}	$apparent\ density\ of\ CaCO_3\ material, kg\ m^{-3}$
ρ_g	$gas\ phase\ density, kg\ m^{-3}$
ρ_s	$apparent\ density\ of\ the\ solids\ mixed\ in\ the\ reactor, kg\ m^{-3}$
η_{cal}	$effectiveness\ factor\ of\ the\ calcination\ reaction, dimensionless$
η_{carb}	$effectiveness\ factor\ of\ the\ carbonation\ reaction, dimensionless$
λ_{eff}	$effective\ axial\ heat\ dispersion\ coefficient\ , W\ m^{-2}K^{-1}$
λ_{0bed}	$effective\ axial\ heat\ dispersion\ with\ no\ flow\ conditions\ , W\ m^{-2}K^{-1}$
τ_i	$time\ for\ complete\ conversion\ when\ using\ gas\ i, s, (i = CO, CH_4\ or\ O_2)$
μ_g	$viscosity\ of\ gas\ , kg\ /\ m\ s$
υ_{CO_2}	$gas - phase\ mole\ fraction\ of\ CO_2\ , dimensionless$
$\upsilon_{CO_2,eq}$	$gas - phase\ equilibrium\ mole\ fraction\ of\ CO_2\ , dimensionless$

*This project has received funding from the European Union's Horizon 2020 research and innovation programme under the Grant Agreement No **884418***